23. Reconstructing the Climatic History of the Western Coast of Africa over the Past 1.5 m.y.: A Comparison of Proxy Records from the Congo Basin and the Walvis Ridge and the Search for Evidence of the Mid-Pleistocene Revolution[1]

E.L. Durham,[2] M.A. Maslin,[2] E. Platzman,[3] A. Rosell-Melé,[4] J.R. Marlow,[5] M. Leng,[6] D. Lowry,[7] S.J. Burns,[8] and the ODP Leg 175 Shipboard Scientific Party[9]

ABSTRACT

A multiproxy approach including the use of stable isotopes, magnetic characterization analyses, and organic geochemistry has been adopted to consider factors such as productivity and terrigenous input over the past 1.5 m.y. at two areas off the western coast of Africa. These factors can, in turn, be used to consider variability in ocean circulation and upwelling in addition to changes in climate on the African continent. In particular, studies focused on the influence of glacial–interglacial cycles and evidence for the mid-Pleistocene revolution (MPR), a complex change in climate that occurred at ~1 Ma. A comparison of the records from the two areas drilled during Ocean Drilling Program Leg 175, the Congo Basin, at a latitude of 5°S (Holes 1076A and 1077A), and the Walvis Ridge, at 17°S (Hole 1081A), demonstrates that these sites are affected by different localized factors. The sites in the Congo Basin are strongly influenced by freshwater and sediment from the Congo River, whereas the site at the Walvis Ridge is located in the center of oceanic upwelling and contains a more marine signal. Evi-

[2]Environmental Change Research Centre, Department of Geography, University College London, 26 Bedford Way, London WC1H 0AP, United Kingdom. Correspondence author: **emma.durham@jncc.gov.uk**
[3]Department of Geology, University College London, Gower Street, London WC1E 6BT, United Kingdom.
[4]Department of Geography, University of Durham, Durham, United Kingdom.
[5]FFEG, Newcastle Research Group, Drummond Building, University of Newcastle, Newcastle upon Tyne NE1 7RU, United Kingdom.
[6]NERC Isotope Geosciences Laboratory, British Geological Survey, Keyworth, Nottingham, United Kingdom.
[7]Geology Department, Royal Holloway, University of London, Egham, Surrey TW20 0EX, United Kingdom.
[8]Stable Isotope Laboratory, Geological Institute, University of Berne, Baltzerstrasse 1, CH-3012 Berne, Switzerland.
[9]Shipboard Scientific Party addresses can be found under **"Shipboard Scientific Party"** in the preliminary pages of the volume.

E.L. Durham et al.
Reconstructing Climatic History

2

dence also suggests that the two sites responded differently to both long- and short-term climatic variations. In particular, the response at the Walvis Ridge to the MPR occurred over an extended period, from 1.1 to 0.8 Ma, and was associated with a change in the dominant source of terrigenous input to the site in conjunction with a change in the productivity signal. In the Congo Basin, the response to the MPR was more rapid, occurring between 0.9 and 0.8 Ma. During this period, the influence of the Congo River became significant. However, productivity records only began to respond toward the end of this interval, at 0.8 Ma.

INTRODUCTION

During Ocean Drilling Program (ODP) Leg 175, 13 sites were drilled off the western coast of Africa from 5° to 32°S latitude (Shipboard Scientific Party, 1998a) (Fig. F1), the tip of southern Africa to the Congo River. This area is the location of the Angola-Benguela Current (ABC) system, a major component of South Atlantic Ocean circulation and one of the greatest upwelling areas of the world (Berger et al., 1998a). The aim of this study is to reconstruct the climatic history along the coast of Africa over the past 1.5 m.y. using a multiproxy approach and, therefore, employing several methods and techniques to obtain records of different proxy indicators. In addition, by comparing records from the two different areas drilled during ODP Leg 175, Sites 1076 and 1077, located in the Congo Basin at a latitude of 5°S, and Site 1081, situated farther south at the Walvis Ridge at 17°S, local vs. global influences can be established.

In particular, records from these areas can be used to consider factors such as the source and supply of terrestrially derived material to the South Atlantic, the compositions and volumes of which may provide evidence for climatic change on the African continent, and the variability and evolution of upwelling and productivity, often assumed to represent a response to changes in the marine environment (e.g., Siesser, 1980; Hay and Brock, 1992). In addition, these two factors may interact; for example, there is evidence for influence of continentally derived iron on marine productivity (Martin, 1992). As a consequence, these records can also be used to consider the coupling and decoupling of marine and continental influences in the area.

Furthermore, by investigating the past 1.5 m.y., it is possible to establish the influence of both long- and short-term climatic variability on the marine and continental environments in addition to determining the influence of the mid-Pleistocene revolution (MPR) and, therefore, to consider the response of the oceans and continents to such climatic fluctuations and events.

Location

The South Atlantic Ocean plays a crucial role in global climate by transferring a huge amount of heat to the North Atlantic (Reid, 1996), and because of this, the South Atlantic is quite different in character from the North Atlantic. The North Atlantic pays for its heat with nutrient deficiency because heat arrives in nutrient-depleted waters (Berger and Wefer, 1996), and the surface waters of the North Atlantic are warm and nutrient poor in comparison to the cold, upwelled, nutrient-rich waters of the South Atlantic. However, evidence suggests that this was

F1. Location of Sites 1075–1087, p. 25.

not always the case and that heat transfer may have been reduced during glacial periods (Raymo et al., 1990; Williams et al., 1998).

The Angola-Benguela Current System

A major component of the heat transfer system from the South Atlantic is the ABC system, which consists of the Angola Current and the Benguela Current (Fig. F2) (Oberhänsli, 1991) and is one of the major upwelling systems in the world. Currently, the cold, nutrient-rich waters of the Benguela Current flow northward, parallel to and within ~200 miles of the coast of southwest Africa. At ~20°S latitude, these waters meet the southward-flowing Angola Current and develop the Angola-Benguela Front (ABF) (Meeuwis and Lutjeharms, 1990). At this front, the Benguela Current is deflected west and merges with the South Equatorial Current.

The present-day latitude of the ABF coincides approximately with the location of the Walvis Ridge. The Walvis Ridge forms a barrier to the northward and southward flow of deep water below 3000 m (Shannon and Nelson, 1996) and effectively separates two areas of intense upwelling. North of the ridge, upwelling and productivity are dominated by Congo River outflow and the Angola Dome, an area of offshore upwelling generated by a sluggish cyclonic gyre formed by the meeting and mixing of the Benguela Current and the Angola Current (Berger et al., 1998a). To the south, wind-driven upwelling interacts with the northward flow of the Benguela Current to create upwelling mainly on the landward side of the current (Berger et al., 1998a).

Studies into the evolution of the Benguela Current demonstrated that it has gradually strengthened since its initiation during the late Miocene (Siesser, 1980), causing it to flow farther north before turning westward and, therefore, shifting its associated upwelling cells northward (Siesser, 1980; Diester-Haass et al., 1992). Hypotheses on the glacial–interglacial variability of the ABC system, however, have proved contentious. Many studies assume that the ABF and the westward deflection of the current shifted north during glacial periods in connection with the global increase in ocean circulation (McIntyre et al., 1976; Jansen et al., 1996), and reconstructions of the last glacial maximum suggested that the current extended into the Gulf of Guinea, or even as far north as the equator (McIntyre et al., 1989). Yet, other studies indicate only a slight intensification of the Benguela Current and a limited shift of the ABF by a few degrees (Jansen et al., 1984; Diester-Haass, 1985), or no significant shift at all (Schneider et al., 1995).

African Continent

Records from the African continent suggest that the continent has suffered a gradual increase in cooling and aridity over at least the past 2 m.y. (Dupont et al., 1989; Tiedemann et al., 1989) in addition to short-term variations in response to glacial–interglacial cycles. The issue of the relative influences of high-latitude global climate change vs. low-latitude local fluctuations in climate is, however, unresolved (deMenocal et al., 1993). The effects of these forcing factors can often be considered in terms of the dominant cyclicities in proxy climate records because high-latitude forcing is attributed to changes in global ice volumes and sea levels and the 100- and 41-k.y. eccentricity and obliquity cycles, whereas low-latitude changes represent changes in precipitation

F2. Large-scale oceanic circulation in the South Atlantic, p. 26.
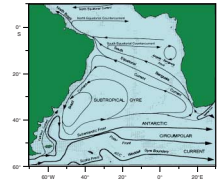
and the monsoons, which have been shown to respond to the 23-k.y. precessional cycle.

Various climatic modeling attempts suggested that tropical climate change over Africa was driven by either one or the other of these factors. For example, pelagic sediments from the eastern equatorial Atlantic showed increased quartz fluxes during glacial periods (Tiedemann et al., 1989), indicating that the African continental climate was more arid during glacial maxima and, therefore, that tropical climate change responded passively to high-latitude climatic change. In contrast, evidence from eastern equatorial sea-surface temperatures (SSTs) showed 23-k.y. periodicities, suggesting the association of upwelling with wind-driven changes in precession (McIntyre et al., 1989) and, therefore, that the South Atlantic and adjacent African continent was driven directly by low-latitude changes. However, deMenocal et al. (1993) ascertained that both these forcing factors have a role to play. Eolian dust and phytolith records from ODP Site 663, located off the northwest coast of Africa, are dominated by 100- and 41-k.y. cycles, yet freshwater diatom records, which provide evidence of lake levels and precipitation, manifest the 23-k.y. cycle.

Location of Sites

Sites 1076 and 1077 are located in the Congo Basin. Hole 1076A is at a shallow-water site, located in 1402 m water depth. The sediments have generally high organic carbon values and consist of olive-gray and greenish gray clays. Sedimentation rates vary between 50 and 210 m/m.y., and there is much evidence of reworked material (Shipboard Scientific Party, 1998c). Hole 1077A sediments are from an intermediate water depth of 2394 m and are composed of greenish gray diatom- and nannofossil-rich clays (Shipboard Scientific Party, 1998d).

A complex environment exists in the Congo Basin, dominated by river input, seasonal coastal upwelling, and incursions from the South Atlantic Ocean (Shipboard Scientific Party, 1998a). The Congo River supplies freshwater, nutrients, and terrigenous material, including freshwater diatoms, phytoliths, and clay minerals, all of which contain evidence of climate change in the drainage basin of the river to the ocean and generated the Congo Fan, which extends for >1000 km into the Angola Basin (Jansen et al., 1984). The fan consists of fairly fine-grained, muddy material, as much of the sandy sediment is trapped in or close to the mouth of the river.

The Walvis Ridge is a basaltic abutment formed from hotspot activity during the Early Cretaceous period (Dean and Gardner, 1985), located at a latitude of 20°S off the coast of Namibia. It extends southwestward from the continental margin for >2500 km toward the Mid-Atlantic Ridge (Shannon and Nelson, 1996). Hole 1081A is at a shallow-water site, located at a 794-m water depth on the ridge. The sediments consist of gray clays with varying amounts of diatoms, nannofossils, foraminifers, radiolarians, and authigenic minerals such as glauconite, pyrite, and dolomite. Sedimentation rates are high and vary from 70 to 150 m/m.y. (Shipboard Scientific Party, 1998e). This site is located directly below the upwelling center on the only topographic high in the area. It provides a comparison with records from ODP Site 532 and Deep Sea Drilling Project (DSDP) Site 362, which are located on the eastern side of the ridge seaward of the upwelling center but contain an upwelling signal that has been transported by the Benguela Current (Shipboard Scientific Party, 1998a).

E.L. Durham et al.
Reconstructing Climatic History

5

The Mid-Pleistocene Revolution

The MPR refers to the transition observed in proxy climatic records from symmetrical low-amplitude, high-frequency (41 k.y.) ice volume variations to high-amplitude, low-frequency (100 k.y.) asymmetrical sawtoothed ice volume variations indicating gradual ice buildup terminated by rapid deglaciation events (Broecker and van Donk, 1970). The MPR resulted in a change in the mean state of the global climate system, including lower global temperatures, increased global ice volume, and lower sea-surface temperatures (Shackleton et al., 1990).

The timing, duration, and cause of the MPR, however, are something of a mystery. The first 100-k.y. cycle in $\delta^{18}O$ records is generally observed at marine isotope Stage 22/23 (0.9 Ma) (Shackleton and Opdyke, 1977). Yet, the classical sawtoothed large-amplitude fluctuations characteristic of the late Pleistocene do not appear until isotope Stage 17 (0.7 Ma) (Shackleton et al., 1990). Studies regarding the timing of the MPR both in terms of its midpoint and the rate of change frequently disagree, and there is evidence to indicate that the MPR may have occurred as early as 1.2 Ma or as late as 0.4 Ma and that its duration was as little as 50 k.y. or as great as 500 k.y. (Prell, 1982; Ruddiman et al., 1989). Yet, it is known that the MPR was a global event, and its occurrence has been documented in both marine and continental records worldwide.

Most importantly, however, the MPR demonstrates that the causal link between insolation and ice volume suggested by Milankovitch (1930; Imbrie et al., 1984) is, in fact, more complex than it first might appear. During the Pliocene and early Pleistocene, it appears that a linear relationship between orbital forcing and ice volume and climatic variations existed (Imbrie et al., 1992). Yet, reconstructions of insolation values (Berger and Loutre, 1991) suggest that there was no significant change in the pattern of insolation at the time of the MPR to account for the transition observed in climatic variations from 41- to 100-k.y. cycles.

Similarly, Imbrie et al. (1993) demonstrated that the amplitude of the 100-k.y. forcing on insolation is at least one order of magnitude smaller than the same insolation signal in the 23- and 41-k.y. bands. Yet, the response of the climate system in these two bands combined is less than one-half the amplitude observed in the 100-k.y. period. Therefore, although the proxy climatic and ice volume records are dominated by the 100-k.y. cycle, the power of the 100-k.y. eccentricity signal on insolation is essentially zero (Shackleton and Opdyke, 1977).

METHODOLOGY

Sample Preparation

Material from Leg 175 was recovered using advanced piston coring, and the retrieved cores were measured in meters below seafloor (mbsf) (Shipboard Scientific Party, 1998b). Upon return to shore, samples were freeze-dried overnight and weighed before subsampling for organic geochemistry analyses, magnetic characterization studies, and stable isotope analysis.

Material for further analysis was sampled at an interval of 0.5 m. Two sites were selected from the Congo Basin because of a paraconformity observed in the Hole 1076A shipboard results at 120 mbsf, indicating

that material below this depth will be difficult to date and interpret. Hole 1076A was therefore sampled at 0.5-m intervals from 0 to 120 mbsf. Hole 1077A was also sampled at 0.5-m intervals from 70 to 160 mbsf. Material from Hole 1081A was sampled every 0.5 m from 0 to 100 mbsf, but with a particular focus on the interval between 40 and 100 mbsf. According to shipboard age-depth models, sampling every 0.5 m provides an age resolution of between 5,000 and 10,000 yr in all three holes.

Stable Isotope Analyses

Samples for stable isotopic analysis were wet sieved through a 63-µm sieve and separated into finer and coarser than 63-µm fractions before oven drying. Foraminifers were picked for isotope analysis from the coarse fraction. To minimize size effects, the samples were also dry sieved through a 250-µm sieve and individual foraminifer tests of each selected specimen were picked from the >250-µm fraction of each sample.

Four planktonic species, *Globigerinoides ruber* (white and pink), *Globigerinoides sacculifer* (with and without sac), *Neogloboquadrina dutertrei,* and *Orbulina universa* were selected for analyses. In addition, the benthic species *Uvigerina peregrina* and a mixed benthic assemblage consisting of mixed *Cibicidoides* taxa were also picked to generate two benthic isotope curves. For each planktonic species, between 10 and 30 individual tests were picked, and for each benthic group, up to 10 tests were picked.

Each foraminifer sample was reacted with phosphoric acid at 90°C in an online automated preparation system, and the resulting carbon dioxide was analyzed on a VG Prism ratio mass spectrometer for both oxygen and carbon isotope ($\delta^{18}O$ and $\delta^{13}C$) values. Corrections for the reaction between the acid and carbonate were applied to the results, and repeated analyses of standard material demonstrated that errors were <0.1‰ for both $\delta^{18}O$ and $\delta^{13}C$. The results were then calibrated to the Peedee belemnite (PDB) scale, according to the NBS-19 standard.

Magnetic Susceptibility

Magnetic susceptibility was measured on discrete samples after return to shore. A small weighed amount of each sample (between 1 and 4 g) was packed tightly into a plastic bag to keep the material cohesive, and the bag was then placed in a small plastic vial. A blank vial was also prepared, containing only an empty plastic bag to allow measurements to be corrected for the containers. Measurements were made on the Kappabridge KLY-2 magnetic susceptibility system. Volume magnetic susceptibility measurements were recorded in 10^{-6} dimensionless SI units and corrected by subtracting the susceptibility of the container. The measurement was then converted to a mass-specific magnetic susceptibility (χ) by dividing the volume susceptibility by the density (mass/volume) of each sample to obtain a measurement in 10^{-6} SI m^3/kg. The volume of each sample was assumed to be 10 cm^3, the volume approximated by the magnetic susceptibility system.

Total Carbon and Total Organic Carbon

Total carbon (TC) concentrations (in weight percent) were obtained on subsamples of dry sediment of known weight (~0.5 g) using a Leco

analyzer, which works by combusting the sample in an electric arc in the presence of oxygen and quantifies the carbon dioxide produced to give percentages of total carbon and total sulfur. A further subsample of sediment was fired at 500ºC for 24 hr to remove organic carbon, and the carbon content was then determined using the Leco analyzer to obtain total inorganic carbon (TIC) concentrations (in weight percent).

The total organic carbon (TOC) content (in weight percent) was determined from the difference between the total carbon and total inorganic carbon concentrations:

$$TOC = TC - TIC.$$

TOC concentration was converted to mass accumulation rate (MAR) to reduce the effects of dilution, using the equation from Emeis et al. (1995):

$$TOC_{MAR} \text{ (mg/cm}^2\text{/yr)} = \text{concentration (wt\%)}$$
$$\times \text{ sedimentation rate (cm/yr)} \times \text{density (g/cm}^3) \times 10.$$

Linear sedimentation rates were calculated from the age-depth models, and gamma ray attenuation (GRA)-derived dry bulk density values were obtained from shipboard records (Shipboard Scientific Party, 1998b).

Organic Geochemistry

The organic material in the sediment was isolated using solvent extraction to investigate its organic components. The analysis was performed at the University of Newcastle, using the procedure based on the methodology of Rosell-Melé et al. (1995), detailed in Figure F3. Weighed subsamples of dried and homogenized sediments were processed partly with a robotic workstation. A known quantity of internal standard (n-C_{32} alkane [dotriacontane]) was added to the samples for later quantification, and the samples were extracted into dichloromethane (DCM) and methanol (3 mL:1 mL). After each extraction, the samples were centrifuged and decanted. The extraction process was conducted five times, until the extracted solvent became colorless. Combined extracts were dried under N_2, leaving a green or yellow residue.

This residue was analyzed first for pigments on the spectrophotometer and then was derivatized with 50 µL of bis(trimethyl)silyltrifluoroacetamide (BST) and 50 µL of DCM before running on the gas chromatograph for lipid analysis.

F3. Process for the extraction of organic matter, p. 27.

Fractionation and Mass Spectrometry

Gas chromatography-mass spectrometry was used to obtain the $U_{37}^{k'}$ index from the C_{37} alkenones (Rosell-Melé et al., 1995). The $U_{37}^{k'}$ index is a measure of the degree of unsaturation of the C_{37} alkenone, which is made up of 37 carbon atoms (Brassell et al., 1986). This index considers the number of di- and tri-unsaturated compounds in the material such that

$$U_{37}^{k'} = [C_{37}:2]/(C_{37}:2+C_{37}:3).$$
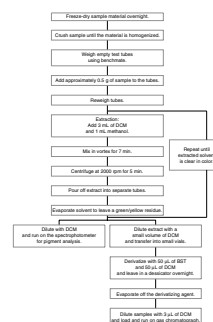
Based on comparisons of laboratory cultures and marine records (Prahl et al., 1988; Prahl and Wakeham, 1987), it has subsequently been demonstrated that this index increases linearly with SST in accordance with the following equation:

$$U_{37}^{k}{}' = (0.033 \times SST) + 0.043.$$

The C_{37}:2 and C_{37}:3 compounds were identified by running the extracted samples on a Carlo Erba gas chromatograph. Quantification was made by gas chromatography with split-splitless injection and flame ionization detection, using an HP 100% polymethylsiloxane column. Hydrogen (H_2) was used as the carrier gas, with a head pressure of 100 kg/cm². The oven temperature program was 45° to 205°C at 20°C/min, 205° to 305°C at 10°C/min, and 305°C for 30 min. Data acquisition and integration were made with an Atlas data system. The alkenones were identified with reference to retention times based on authenticated standards, and the results were quantified using the internal standard. Peak areas were used to calculate the $U_{37}^{k}{}'$ index, from which SSTs were then estimated using the standard equation of Prahl et al. (1988).

Pigment Analysis

The chlorins and porphyrins in the solvent extracts of the sediments were identified using electronic spectrophotometry on a Philips PU8730 spectrophotometer. The residues of the extracted samples were diluted with between 5 and 15 mL of DCM, depending on their color. When the diluted sample yielded a pale yellow color, 3 mL of the liquid was poured into a cuvette and placed in a diode array spectrophotometer, which scans in the ultraviolet (UV)-visible wavelength interval (350–850 nm). The relative abundances of the chlorins and porphyrins were estimated by measuring the absorbance of the extracts in the regions close to the Soret band (S), which has highest extinction in the near-UV range (360–420 nm), and the Satellite band (I), close to 665 nm.

The relative absorbance value of the chlorinlike pigment (at 665 nm) was recalculated to give concentration values per gram as follows:

$$Concentration/g = (absorbance \times dilution\ factor)/mass.$$

In addition, raw chlorin concentrations (in micrograms per gram) were converted to mass accumulation rates using the calculation from Emeis et al. (1995), according to the linear sedimentation rate calculated from the age-depth models and density measurements from GRA-derived dry bulk density values from shipboard records (Shipboard Scientific Party, 1998b), as follows:

$$Chlorin\ MAR\ (\mu g/cm^2/yr) = concentration\ (\mu g/g)$$
$$\times\ sedimentation\ rate\ (cm/yr) \times density\ (g/cm^3).$$

In the modern oceans, it has been established that phytoplankton productivity can be estimated from the concentrations of chlorophyll in seawater (Harris et al., 1996). Chlorophyll is the main pigment used in photosynthesis by higher plants and algae, which produce several pigmented organic compounds (Meyers, 1997). Chlorophyll, however, is not preserved in sediments, but chlorins and porphyrins, which are

E.L. Durham et al.
Reconstructing Climatic History

9

the transformation products of chlorophyll, are. Chlorins are the immediate diagenetic products of chlorophyll, whereas porphyrins result from long-term chlorophyll diagenesis (Rosell-Melé and Koç, 1997). Chlorin accumulation rates, calculated from density and sedimentation rates, have subsequently been shown to be a reliable and taxonomically independent indicator of paleoproductivity in areas of upwelling near Africa (Harris et al., 1996).

The ratio of the concentrations or absorbances at wavelengths of 410 and 665 nm can also be used to classify the pigments. By assuming that chlorinlike pigments have a wavelength close to 665 nm, whereas porphyrinlike pigments are represented by the 410-nm wavelength, it has been shown that chlorin-rich sediments have a 410/665 (porphyrin/chlorin) ratio between 1 and 5, whereas porphyrin-rich sediments have a higher value, between 5 and 10 (Rosell-Melé and Koç, 1997; Rosell-Melé et al., 1994).

CONSTRUCTION OF AGE-DEPTH MODELS

Age-depth models were constructed for each hole to translate depth measurements to age measurements. At all sites, age-depth models were constructed based on preliminary shipboard biostratigraphy and magnetostratigraphy. These models were then constrained using oxygen-isotope stratigraphy, where oxygen-isotope ($\delta^{18}O$) data was available, by comparing the $\delta^{18}O$ records from the sites with the standard $\delta^{18}O$ curve from Tiedemann et al. (1994). To infer the age at every sample depth, a constant sedimentation rate between dated depth points was assumed.

Hole 1076A

The shipboard age-depth model based on nannofossil horizons suggests a disagreement between the biostratigraphy and magnetostratigraphy between 90 and 120 mbsf (Shipboard Scientific Party, 1998c). Biostratigraphic data indicates that the core extends to beyond 1.0 Ma, yet there is no evidence for the Brunhes-Matayama polarity reversal, dated at 0.78 Ma, in the magnetic records (Berggren et al., 1995; Shipboard Scientific Party, 1998c).
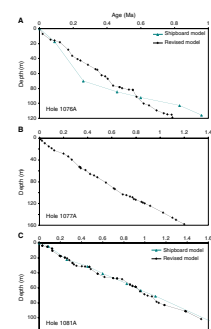
The age-depth model for Hole 1076A was first constructed using the preliminary shipboard biostratigraphic data and subsequently revised using $\delta^{18}O$ records from the benthic foraminifer *U. peregrina*, which were compared with the standard $\delta^{18}O$ record from Tiedemann et al. (1994). The revised age-depth model, in fact, suggests that the upper 120 m of the core may not extend beyond 0.78 Ma and, therefore, that the shipboard biostratigraphic data may be incorrect.

Age-depth points established by correlation with the standard $\delta^{18}O$ curve of Tiedemann et al. (1994) are shown in Table T1, and age-depth points from shipboard data are provided in Table T2. The two age-depth models are plotted in Figure F4A. Comparison of the two models suggests that ages are older than biostratigraphic data in the interval from 19 to 94 mbsf, yet below this depth, ages are younger than the shipboard model. The good correlation between the standard $\delta^{18}O$ curve from Tiedemann et al. (1994) and the $\delta^{18}O$ curve generated for Hole 1076A, which also agrees with shipboard magnetostratigraphic data, suggests that the age-depth model can be assumed to be reliable until at least 94 mbsf (0.6 Ma), yet beyond this depth some caution should be taken in interpreting the results.

Hole 1077A

Because of the paraconformity in Hole 1076A at 120 mbsf, material was obtained from Hole 1077A to construct a record from the Congo Basin that extends to at least 1.2 Ma. The age-depth model for Hole 1077A was obtained from L.M. Dupont et al. (unpubl. data) and was generated using $\delta^{18}O$ data from the hole and oxygen isotope stratigraphy. The age-depth points used to constrain the model are shown in Table T3. This age-depth model is plotted in Figure F4B.

Hole 1081A

The age-depth model for Hole 1081A was initially constructed using shipboard biostratigraphic horizons and then constrained using oxygen isotope stratigraphy and comparison with the standard $\delta^{18}O$ curve of Tiedemann et al. (1994). The $\delta^{18}O$ records from the benthic foraminifer species *U. peregrina* and the planktonic species *N. dutertrei* were used for this comparison.

Shipboard records suggest that foraminifer abundance decreased greatly below 105 mbsf, yet the isotopic record only extends downcore to ~90 mbsf. Below this depth, shipboard ages and linear sedimentation rates were used to date the material. Additionally, there is evidence for some foraminifer-poor intervals in the upper 105 m of the record. Age-depth points are provided in Table T4, and age-depth points from the shipboard biostratigraphy data are given in Table T5. Both models are displayed in Figure F4C.

RESULTS AND DISCUSSION

Records generated from the Congo Basin and the Walvis Ridge provide an insight into the dominant climatic and marine factors that influenced these areas. These factors include the influence of both gradual changes, the MPR, and short-term glacial–interglacial variability. A synthesis of the main events is provided in Figures F5 and F6.

Terrigenous Input

A comparison of several proxy indicators of terrestrially derived supplies of material to the Congo Basin and the Walvis Ridge supports the use of the magnetic susceptibility record as a reliable indicator of terrigenous input (Durham, 2000). Magnetic susceptibility measures the concentration of magnetizable material in the sediment and the ease with which it can be magnetized (Thompson and Oldfield, 1986). In deep-sea sediments, this material is predominantly terrigenous in origin, as biogenic components are diamagnetic and therefore effectively non-magnetic. Magnetic susceptibility varies according to the size and source of the lithogenic supply to the ocean and the biogenic/lithogenic ratio of the deep-sea sediments, both of which are essentially climatically controlled (Kent, 1982).

Further evidence for terrigenous input comes from low-resolution shipboard X-ray diffraction (XRD) data (Shipboard Scientific Party, 1998b). The identification and partial quantification of minerals by XRD enables an estimation of the relative abundances of materials such as quartz and clay minerals.

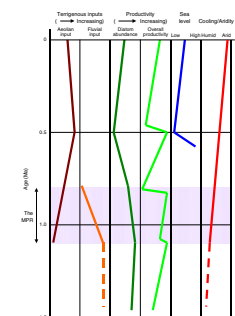T3. Oxygen-isotope stratigraphy age-depth data, Hole 1077A, p. 44.

T4. $\delta^{18}O$ age-depth data, Hole 1081A, p. 45.

T5. Biostratigraphic horizon age-depth data, Hole 1081A, p. 46.

F5. Overall transitions in fluvial terrigenous input, productivity, and aridity, p. 29.
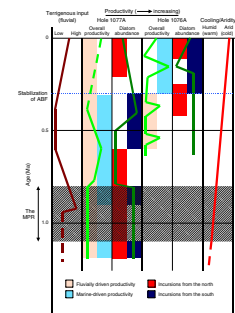
F6. Overall transitions in terrigenous input, productivity, and sea level and aridity, p. 30.

In particular, quartz is continentally derived and, therefore, can be used as an indicator of terrigenous input (Tiedemann et al., 1989). In addition, it is often attributed to eolian input and has therefore been used in some studies as an indicator of dust flux to the deep sea from the continents (Tiedemann et al., 1989), enabling a consideration of aridity and wind strengths. Clay minerals are also major constituents of deep-sea sediments and have a predominantly continental origin. Their distribution in the oceans is related to the sources and transport paths of material from the continents, influenced by climatic regimes and weathering processes (Singer, 1984). In particular, the clay mineral kaolinite has been shown to be associated with aridity–humidity variations (Singer, 1984). Because kaolinite is a known product of chemical weathering of igneous rocks in the tropical rainforest, enhanced supplies of kaolinite are generally assumed to represent increases in humidity. However, kaolinite volumes might also increase if overall supply is increased, and therefore, the relative amount of kaolinite compared to the supply of smectite is more favorably employed as an indicator of aridity and humidity by using kaolinite/(kaolinite+smectite) values (Singer, 1984).

In addition, comparison of the volumes of chlorins vs. porphyrins (the 410/665 porphyrin/chlorin ratio) in marine sediments can be used to consider sources of material and has been shown to be an indicator of terrigenous input (Rosell-Melé and Koç, 1997). A typical marine 410/665 signal in recent material would be expected to show a gradual increase in values downcore as chlorins gradually degrade to porphyrins with time and push the ratio upward. However, if the record shows great variability or high porphyrin/chlorin ratios, this suggests that there has been an input of porphyrins from another source. Often, this has been attributed to the input of degraded continental organic matter (Rosell-Melé and Koç, 1997).

Congo Basin

Terrigenous input to the Congo Basin is predominantly driven by input from the Congo River (Jansen et al., 1984; Durham, 2000). Support for the use of the magnetic susceptibility record as an indicator of terrigenous input and, in particular, fluvial flow from the Congo River comes from studies that show that the majority of material transported by the river is fine-grained paramagnetic clay (Frederichs et al., 1999). Concentrations of paramagnetic materials have a large influence on magnetic susceptibility values, particularly in areas where supplies of other magnetic materials are low (Thompson and Oldfield, 1986).

Sedimentation rates in Holes 1076A and 1077A are high compared to those usually observed in deep-sea sediments (Shipboard Scientific Party, 1998a). Sedimentation rates are often assumed to reflect variability in terrigenous supplies (Schneider et al., 1997), especially in areas where terrigenous input is high and variable, yet these rates can also be influenced by supplies of organic matter in areas where productivity is high (Stein et al., 1989). The material from Holes 1076A and 1077A, which contains high volumes of both terrestrially derived clays and organic matter, suggests that enhanced sedimentation rates in this area are the result of both large volumes of terrigenous material from the Congo River and high productivity (Durham, 2000).

Hole 1076A sedimentation rates vary between 20 and 450 m/m.y. with an average of 215 m/m.y., whereas Hole 1077A rates vary between 40 and 280 m/m.y. with a lower average of 116 m/m.y. (Durham, 2000).

The higher rates for Hole 1076A may be a result of its proximity to the mouth of the Congo River, causing it to receive enhanced supplies of fluvially derived terrigenous material compared to its more distal neighbor. In addition, Hole 1077A sedimentation rates suggest a change in source or supply between 0.8 and 0.9 Ma. Prior to this, values average ~100 m/m.y. and there is very little variability.

Shipboard and shore-based magnetic susceptibility records from both Holes 1076A and 1077A compare favorably with one another and provide evidence for glacial–interglacial variability, with increased values coinciding with interglacial periods (Figs. F7, F8), indicating that terrigenous input was enhanced during interglacial periods. In conjunction with this, previous studies on the Congo Fan demonstrated that the flow of the Congo River increased during periods of enhanced humidity, coincident with warm interglacial periods (Jansen and van Iperen, 1991).

In addition, there is evidence for intermittent increases in magnetic susceptibility values during glacial periods (Durham, 2000; L.M. Dupont et al., unpubl. data). It has been suggested that these increases during glacial periods provide evidence for lower sea levels and enhanced erosion of the continental shelf (L.M. Dupont et al., unpubl. data). These increases are more evident in the records of Hole 1077A, suggesting that they may be a result of its more distal nature from the river mouth, causing it to receive greater influxes of terrestrial material from other sources.
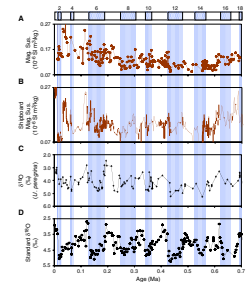
In addition, the 410/665 ratio record for Hole 1077A compares favorably with the magnetic susceptibility record (Fig. F9) and therefore supports the use of both these parameters as indicators of terrigenous input.

Spectral analysis on the magnetic susceptibility records provides evidence for cycles with periods, indicative of Milankovitch forcing factors (Durham, 2000). In particular, a cycle with a periodicity close to 100 k.y. has been identified in Hole 1077A in both shipboard and shore-based magnetic susceptibility records. In addition, both sites display evidence for strong cycles in the precessional band. The existence of strong cycles in this band supports the suggestion that the production of sediment in the Congo Basin, which controls the sediment load of the Congo River, is driven by low-latitude precessional forcing (Berger et al., 1998b), which may affect aridity and humidity. The presence of a 100-k.y. cycle in Hole 1077A provides evidence for high-latitude forcing and may represent the supply of terrestrial material to this site due to the redistribution of sediment from the continental shelf in association with 100-k.y. variability in sea level changes.

In support of the hypothesis that glacial–interglacial variability in the magnetic susceptibility records is driven by fluctuations in fluvial flow, several previous studies demonstrated that during glacial periods the African continent suffered increased aridity, causing decreased flow of the Congo River (Jansen and van Iperen, 1991; Pastouret et al., 1978). Vegetation reconstructions have also demonstrated that during the last glacial maximum, the drainage basin of the Congo River consisted of savanna and grassland and the coastal zone was a desert, indicative of an arid environment, whereas in the present day, the same area is covered by woodland and tropical rainforests (Jansen and van Iperen, 1991).

Long-term trends in the magnetic susceptibility records provide evidence for a gradual decrease in terrestrial input from 0.9 to 0.4 Ma in Hole 1077A and from the base of the record (0.75 Ma) to 0.4 Ma in Hole
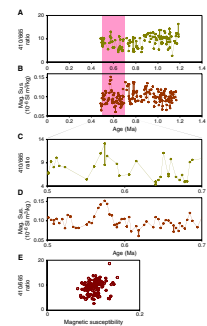
F7. Magnetic susceptibility and δ18O curves, Hole 1076A, p. 31.

F8. Magnetic susceptibility and δ18O curve, Hole 1077A, p. 32.
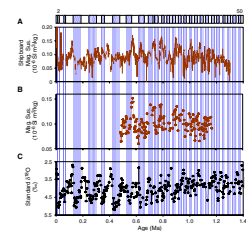
F9. The 410/665 ratio and magnetic susceptibility, p. 33.

1076A. In the upper 0.4 Ma of the record, values begin to increase (Figs. F5, F8, F9). In addition, values for Hole 1076A are very low from 0.6 to 0.4 Ma, suggesting that fluvial flow reached a minimum at 0.6 Ma. In support of this, records of quartz concentrations show similar variability (Fig. F10). A decreasing trend in quartz values is particularly evident in Hole 1076A from the base of the core to 0.4 Ma, although, in fact, a further small decrease in quartz is also evident until 0.3 Ma. A decreasing trend also occurs from 0.9 to 0.4 Ma in the quartz records for Hole 1077A.

These records suggest that terrestrial input to the Congo Basin gradually decreased from at least 0.9 to 0.4 Ma. This can be attributed to a response to overall increased aridity, which has been shown to have occurred during the Quaternary period (Dupont et al., 1989; Tiedemann et al., 1989). This increase in aridity may have reduced the flow of the Congo River and, therefore, its sediment load. This signal was interrupted, however, at 0.4 Ma, when terrestrial input began to increase. In addition, a change in sediment supply to the Congo Fan was observed at this time (Jansen et al., 1984). Jansen et al. (1984) suggest that this may represent a response to a localized increase in humidity in the drainage basin of the river, but insufficient evidence from land records is available to justify this hypothesis.

In conjunction with this transition in trends, glacial–interglacial cyclicity demonstrates that sediment supply continued to increase during interglacial periods, suggesting that supply was still driven by the river. This increased supply, therefore, could represent a local increase in humidity, as suggested by Jansen et al. (1984), although it may also represent a response to the continuing increase in aridity, which may cause reduced vegetation cover, enabling more erosion and a greater source of material. Therefore, although the flow of the river may have decreased, its sediment load may have increased in response to a greater availability of material (Durham, 2000).

A similar event occurred at 0.9 Ma. Prior to 0.9 Ma, records from Hole 1077A demonstrate that fluctuations in the amplitude of quartz concentrations and quartz values are low. In addition, magnetic susceptibility values are also low and sedimentation rates manifest little variability, suggesting that supply from the Congo River may have been less significant at this time. At 0.9 Ma, increases in magnetic susceptibility and quartz values occur prior to the gradual decreasing trend. In addition, a large drop in the kaolinite/(kaolinite+smectite) record is evident. The change in these records coincides with the timing of the MPR. In many locations, this event has been associated with an increase in aridity, which, in a similar fashion to the event at 0.4 Ma, may have caused the sediment load of the Congo River to increase, although its flow may have been reduced. In support of this, pollen reconstructions from Hole 1077A (L.M. Dupont et al., unpubl. data) suggest that a change in vegetation occurred between 1.0 and 0.9 Ma.

Walvis Ridge

The terrigenous input signal inferred from Hole 1081A shipboard and shore-based magnetic susceptibility records over the past 0.8 Ma on the Walvis Ridge is quite typical of the signal that would be expected at such a location far from fluvial influences (Fig. F11). Input increased during glacial periods in association with global cooling and enhanced aridity, leading to an increase in the supply of eolian material. Eolian transport from the Namib desert by northeasterly to easterly winds is

F10. Quartz concentrations and (k/[k+sm]), Holes 1076A and 1077A, p. 34.
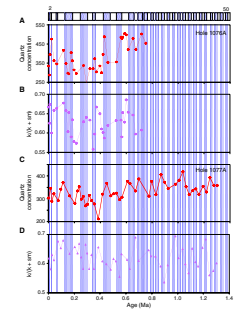
F11. Magnetic susceptibility, $\delta^{18}O$ curves, and SST, Hole 1081A, p. 35.
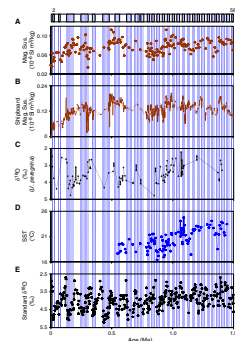
corroborated by wind erosion forms (Diester-Haass et al., 1988). In addition, the lowering of sea levels in response to global cooling and increased ice volume during glacial periods left greater areas of the continental shelf and slope exposed and vulnerable to erosion and, therefore, also able to provide supplies of terrestrial material.

Diester-Haass and Rothe (1987) further argued from clay mineralogy evidence at DSDP Site 532 that a supply of terrigenous material from the Orange River, located to the south at a latitude of 28°S, may have reached the Walvis Ridge during glacial periods. Over the past 0.7 m.y., therefore, the supply of terrigenous material to the ridge was increased during glacial periods, not only by eolian input and reworking of material from the continental shelf, but also by a supply from the Orange River from the south, transported to the ridge by the intensified strength and flow of the Benguela Current (Meeuwis and Lutjeharms, 1990).

The opposite terrigenous signal, however, is evident in the last 1–1.5 m.y., and a change in mineralogy suggests that a change in conditions occurred between 1.1 and 0.8 Ma. In contrast to increased terrigenous input during glacial periods, from 1.5 to 1.0 Ma, terrigenous input increased during interglacial periods. This suggests that the supply of terrigenous material via eolian input may only have been significant at the Walvis Ridge in the last 0.8 m.y., suggesting that prior to this period a different source of terrigenous material played a major role.

Evidence from mineralogy provides support for an additional or different source of terrestrial material influencing the ridge from 0.8 to 1.5 Ma (Fig. F12). During this period, quartz concentrations decreased and kaolinite values increased. Yet, subsequent to this, the values appear to parallel one another and both manifest an overall decreasing trend from 1.0 to 0.8 Ma. Diester-Haass and Rothe (1987) suggested that kaolinite was a major constituent of the Kunene River, located north of the Walvis Ridge at 17°S, but was not evident in the material from the Orange River. In addition, it has been demonstrated that the ABF, which controls the latitude at which the Benguela Current turns west, also controls the southerly extent of the southward-flowing Angola Current (Jansen et al., 1996). It has been shown that this front shifted further north during glacial periods (Jansen et al., 1996). Therefore, during interglacial periods in the 1.0- to 1.5-Ma period, the ABF may have been far enough south to allow the supply of terrigenous matter from the Kunene River to be transported via the Angola Current to the Walvis Ridge.

Kaolinite concentrations, however, dropped significantly between 1.1 and 0.8 Ma. Although kaolinite is a measure of humidity, supplies are also strongly dependent on source (Frederichs et al., 1999; Diekmann et al., 1999), and this evidence suggests that between 1.1 and 0.8 Ma the supply of material from the Kunene River via the Angola Current from the north was somehow reduced and was therefore no longer observed at the ridge after 0.8 Ma. This change in supply may be attributed to one of two possible factors, or even both (Durham, 2000)—either that the Angola Current no longer reached the ridge subsequent to this time or that the flow and terrestrial supply from the river was greatly reduced because of increased aridity, meaning that although the Angola Current may have continued to reach the ridge, it no longer brought with it a supply of terrigenous material.

In support of this second factor, Oberhänsli (1991) suggested that intermittent incursions of the Angola Current are evident at the Walvis Ridge over the past 0.5 m.y. This suggests that it is the supply of the

F12. Magnetic susceptibility, quartz, kaolinite, and smectite, and (k/[k + s]), Hole 1081A, p. 37.

E.L. Durham et al.
Reconstructing Climatic History

15
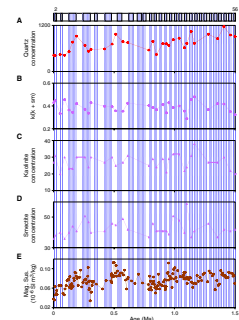
river, rather than the influx of the current, that caused this change in source (Durham, 2000). The timing of this change in supply and source of terrigenous input to the Walvis Ridge coincided with the timing of the MPR. In addition, it has been shown that aridity on the African continent significantly increased between 1.1 and 0.9 Ma (L.M. Dupont et al., unpubl. data), and this may have caused a decrease in the flow of the river.

Subsequent to this event, magnetic susceptibility values gradually increased until 0.5 Ma, after which values decreased. The increasing trend in values in conjunction with increased supplies during glacial periods indicates a response to increased aridity, causing an increase in eolian input due to enhanced exposure of the continent and the continental shelf and increased erosion, both on long and short timescales. The termination of this trend at 0.5 Ma, however, indicates that the supply of material began to decrease, although evidence from mineralogy does not indicate a change in source. This may, therefore, perhaps represent a response to several possible factors, including a gradual decrease in the supply of material from the exposed continental shelf in association with a gradual increase in sea levels, a decrease in wind strengths, or even a decrease in the volume of material eroded due to a decrease in humidity-related chemical weathering.

Productivity and Upwelling

Comparison of several productivity proxy records demonstrates that the most reliable indicator appears to be the chlorin MAR and TOC MAR records. Although these are dependent on sedimentation rate, the close correlation between chlorin MAR and chlorin concentration evident from scatter plots indicates that, in fact, sedimentation rate appears to be highly driven by organic matter and, therefore, that the influence of terrigenous supply on these mass accumulation rates can be ignored (Fig. F13). In addition, evidence from the shipboard evidence for the fossil assemblages may also help us consider the dominant primary producers and dominant water masses and sources (Shipboard Scientific Party, 1998c, 1998d, 1998e).

Congo Basin

Upwelling in the Congo Basin is not directly related to the Benguela Current, which does not travel as far north as the basin (Jansen and van Iperen, 1991). Instead, the shifting north of the ABF means that incursions and eddies of upwelled water, associated with the Angola Dome, formed by the ABF, may be seen in this area (Jansen et al., 1996). In addition, over the past 0.2 m.y., southerly excursions of the ABF led to the influence of equatorial doming from the north in the waters overlying the Congo Fan (Peterson and Stramma, 1991; Jansen et al., 1996). The location of the fan and Holes 1076A and 1077A, situated north of the fan, means that they are, therefore, sensitive to the influence of two thermal domes, the equatorial dome to the north and the Angola Dome to the south. Incursions from these domes are associated with the northerly and southerly shifting of the ABF (Peterson and Stramma, 1991; Jansen et al., 1996).

Previous studies also demonstrated that, in general, the nutrient supply from the Congo River to the ocean is greater during humid (interglacial) rather than arid (glacial) periods, yet periods with more variable river fluxes and high coastal upwelling coincide more often with arid

F13. Chlorin MAR vs. chlorin concentration, p. 38.
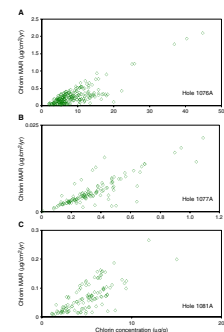
periods (Jansen and van Iperen, 1991). High biological productivity off the Congo River is characterized by very high diatom productivity, evident in a plume that reaches out into the open ocean for 800 km (van Bennekom and Berger, 1984; Schneider et al., 1997). In association with this plume, river-induced upwelling has also been shown to occur (Jansen and van Iperen, 1991).

Records from Holes 1076A and 1077A indicate that no clear glacial–interglacial variability in productivity is evident in the Congo Basin (Figs. F14, F15). The first evident peak in the productivity record from Hole 1077A occurs at 1.1 Ma during interglacial Stage 37, and a subsequent peak occurs at 0.98 Ma during Stage 31. Throughout this interval until 0.8 Ma, upwelling diatoms are high in abundance and evidence from foraminifers suggests that waters from the north were apparent above Hole 1077A from 1.2 to 0.6 Ma (Shipboard Scientific Party, 1998d; Durham, 2000). In addition, influxes of colder waters from the south occurred between 1.2 and 1.05 Ma and 0.88 and 0.8 Ma. The incursion between 0.88 and 0.8 Ma may be the cause of the low SSTs evident at this time; SST values in the 1.2- to 0.5-Ma interval are also slightly reduced (Fig. F15).

The productivity peaks at 1.1 and 0.98 Ma, therefore, occur when warm waters from the north are evident in Hole 1077A, although the peak at 1.1 Ma also coincides with an influx of waters from the south. Both coincide with increased terrigenous input, suggesting a fluvial influence (Durham, 2000). The influx of water from the south at 1.1 Ma does not influence this river-induced signal, yet a small increase in productivity in the glacial period prior to the event at 1.1 Ma (isotope Stage 32) may represent enhanced marine upwelling due to this incursion.

At 0.8 Ma, records from Hole 1077A show a decrease in the abundance of upwelling diatoms in conjunction with an increase in productivity, which is enhanced intermittently in both glacial and interglacial periods (Fig. F15). From 0.8 to 0.6 Ma, the area remained bathed in waters from the north, with no evidence of waters from the south. The increases during interglacial periods suggest the influence of the river. Yet, the lack of evidence for waters from the south indicates that the glacially induced productivity during this interval was not driven by southern waters and was, instead, driven by other marine forces such as enhanced coastal upwelling. A brief decrease in productivity coincides with an influx of the warm-water foraminifer *G. ruber* between 0.75 and 0.65 Ma, suggesting an enhanced incursion of warm waters from the north, may have temporarily impeded these influences.

From 0.6 to 0.4 Ma, productivity in Holes 1076A and 1077A was low, except for a peak at both sites at 0.56 Ma toward the end of interglacial Stage 15 and a further peak at 0.42 Ma in Hole 1076A. Both appear to have a fluvial driving force (Durham, 2000). During this interval, incursions of water from the south are again evident in Hole 1077A. In addition, there is no evidence for incursions from the north, suggesting either that northern waters were cut off by the enhanced strength of the southerly waters or that the southerly waters reached the site because of the reduced flow of the river or even that the strong current from the south may have impeded the flow of the river (Durham, 2000).

At 0.4 Ma, upwelling diatoms increase in abundance in Hole 1077A, foraminifers become abundant in Hole 1076A, and terrigenous input at both sites begins to increase, suggesting sediment supply from the river was enhanced. Foraminifer assemblages from Hole 1076A indicate that an incursion of water from the north occurred at this time and the trop-

F14. Chlorin MAR, TOC MAR, and magnetic susceptibility, Hole 1076A, p. 39.
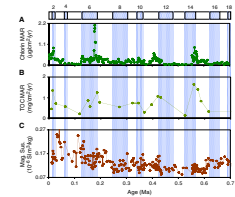
F15. Chlorin MAR, TOC MAR, SST, and magnetic susceptibility, Hole 1077A, p. 40.
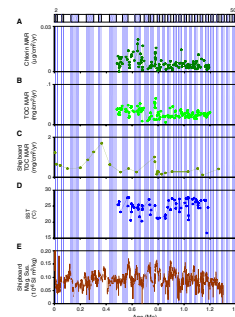
ical species *G. ruber* is also briefly evident, yet productivity is low, and in Hole 1077A, waters from the south remained dominant. At 0.3 Ma, it has been proposed that the position of the ABF stabilized (Shipboard Scientific Party, 1998d, 1998e). After this time, the influence of southern waters appears to have ceased in Hole 1077A, and from 0.24 Ma, there is once again evidence for warmer waters from the north.

In Hole 1076A, incursions of waters from the south began at 0.2 Ma and the influence of northern waters ceased between 0.25 and 0.05 Ma. Therefore, despite its more southerly location, the influence of waters from the south is not evident in Hole 1077A, suggesting that although the ABF shifted to the north and stabilized, the transport of waters from the south to Hole 1077A was somehow impeded (Durham, 2000). In the upper 0.2 m.y. of Hole 1076A, the most evident productivity event occurs at 0.18 Ma, and there is also evidence for such an event in studies from the Congo Fan (Jansen and van Iperen, 1991; Jansen et al., 1996). Yet, this event is not evident in Hole 1077A, suggesting that different water masses affected the two sites at this time. The event has been attributed to a temporary shifting of the ABF to the south and the influence of equatorial doming (Jansen et al., 1996).

The evolution of the productivity records from Holes 1076A and 1077A, therefore, demonstrates that a complex interaction of factors drives productivity records in this region. In Hole 1077A, enhanced productivity is not as extensive in either duration or magnitude as in Hole 1076A, yet there is evidence for more frequent periods of increased productivity, particularly during interglacial periods. In addition, interglacial productivity appears to coincide with enhanced supplies of terrigenous input, suggesting that it was driven in part by the Congo River. Yet, glacial increases in productivity cannot be so simply attributed to one source, as at times they coincide with incursions of waters from the south, whereas at other times, there is no clear evidence for other water masses and a wind-driven coastal upwelling cause is hypothesized (Durham, 2000).

The record for Hole 1076A shows less consistent variability and is dominated by four major productivity events. In addition, the close proximity of the site to the Congo River might suggest that it would be more highly driven by fluvially driven nutrient input, but although it received an enhanced sediment load from the river, it does appear to be located at the very edge of the nutrient-enriched plume and, therefore, was less affected by fluvially induced productivity than Hole 1077A, which, although at a more distal location from the river mouth, was more greatly influenced by the plume. In addition, the proximity of Hole 1076A to the continent means that it was also less affected by marine-induced productivity than Hole 1077A and, therefore, that its productivity record represents responses to significant transitions or events in both the marine and terrestrial environment, rather than a consistent response to gradual or cyclic changes.

Walvis Ridge

Previous evidence from the Walvis Ridge has proved to be contentious over the issue of glacial–interglacial cyclicity because it has been argued by several authors (Oberhänsli, 1991; Summerhayes et al., 1995; Little et al., 1997) that upwelling at the latitude of the Walvis Ridge generally increased during glacial periods, whereas other studies suggest that upwelling was more intense during interglacial periods (Diester-Haass, 1985).

It has since been suggested, however, that the discrepancy between these records may not necessarily reflect a decrease in upwelling and productivity during glacial periods but could instead be an artifact of the location of the site (Diester-Haass et al., 1992) and, therefore, that upwelling may have been enhanced during glacial periods but that the signal may have been transported elsewhere. Alternatively, it has been hypothesized that upwelling persisted but that the upwelled water was depleted in nutrients because of changes in deep-sea circulation (Hay and Brock, 1992). In a similar fashion, Oberhänsli (1991) suggests that the site did experience intensified productivity from increased upwelling during glacial periods but this was not reflected in some records because of poor preservation.

Records from Hole 1081A generally provide evidence for increased productivity during glacial periods (see Fig. F16). A peak occurs in all proxy records of productivity at 1.1 Ma that coincides with a maximum in diatom abundance. Subsequent to this, diatom abundance dramatically decreases, the abundance of foraminifers begins to increase, and values in other productivity proxies remain elevated (Durham, 2000). This change in the dominant microfossil species might suggest that a temperature-associated threshold (Hay and Brock, 1992) was reached at this time, causing diatom productivity to begin to deteriorate, whereas overall productivity remained high until 0.8 Ma when values significantly drop in association with a more rapid decrease in diatom abundance. This diatom maximum has, in fact, been observed in many records from the South Atlantic and is followed by a decrease in abundance that begins between 1.5 and 1.0 Ma (Dean and Parduhn, 1984; Berger and Wefer, 1996), suggesting it is driven by more than just localized variability.

The timing of these changes in productivity suggests that they may be related to the MPR. In association with this event, hypothesized to have caused increased cooling and aridity in this area (L.M. Dupont et al., unpubl. data), it is possible that the water masses or nutrient supplies began to gradually change, causing diatom productivity to begin to decrease following a period of elevated and increasing values, while productivity continued to be elevated. At 0.8 Ma, a significant and rapid drop in both overall productivity and diatom abundance is evident, suggesting that the gradual change was complete.

From 0.8 to 0.5 Ma, productivity begins to increase once again and diatom abundance decreases more rapidly, culminating in a disappearance in diatoms at 0.5 Ma in association with a peak in productivity. Productivity then appears to rapidly drop before gradually recovering in the latest 0.4 m.y. in conjunction with a gradual increase in diatom abundance. Studies suggested that an abrupt decrease in sea level may have occurred at this time (Vail et al., 1977; Haq et al., 1987; van Donk, 1976), and this may have been the cause of this rapid increase and subsequent decrease in productivity at 0.5 Ma. In response to a sea level drop, productivity may be enhanced, as lowered sea level means that nutrient-enriched bottom waters are closer to the surface and also that there is less volume of water in which the nutrients are distributed (Hay and Brock, 1992). The peak is, however, only short-lived, suggesting that the enhanced productivity removed the nutrients before they could be replaced, and productivity, therefore, subsequently rapidly decreased. The gradual subsequent increase in productivity values following this decrease indicates that conditions begin to return to normal as sea level began to rise and nutrient supplies were replaced.

F16. Chlorin MAR, TOC MAR, SST, and magnetic susceptibility, Hole 1081A, p. 41.
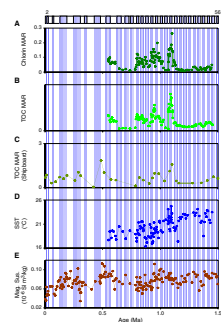
Evidence for the MPR

The influence of the MPR is evident in the records from both the Congo Basin and the Walvis Ridge, although its impact on these areas was different. In particular, the effect of the MPR at the Walvis Ridge was more gradual, especially in proxy productivity records (Durham, 2000).

Proxy productivity records from the Congo Basin show a very rapid change at 0.8 Ma, suggesting that the basin responded only when conditions had fully changed. A brief incursion of waters from the south is, however, apparent from 0.9 to 0.8 Ma (Fig. F5), which might suggest that the strength of the Benguela Current intensified at this time, but lack of further evidence for southern waters until much later in the record indicates that this incursion was only temporary. In addition, however, there is evidence for enhanced glacial productivity subsequent to 0.8 Ma, indicating that either coastal or marine upwelling was enhanced in conjunction with increased productivity associated with the flow of the river.

Evidence from terrigenous input to the Congo Basin suggests that the MPR occurred between 1.0 and 0.9 Ma and may have caused a decrease in the flow of the Congo River (L.M. Dupont et al., unpubl. data). Yet, in conjunction with this, the sediment load of the river appears to increase (Durham, 2000). In addition, subsequent to this event, productivity was enhanced, and this, too, may be attributed to an increase in the nutrient load of the river after this time.

At the Walvis Ridge, the MPR appears to have occurred more gradually between 1.1 and 0.8 Ma and caused a change in the dominant source of terrigenous material to the ridge in conjunction with a change in productivity. It is hypothesized that these events are connected (Durham, 2000) and that prior to the MPR, a supply of terrigenous material from the Kunene River, situated north of the ridge, may have been transported to the ridge by the Angola Current and partially driven productivity. The MPR appears to result in a decrease in the flow and sediment load of this river, however, as subsequent to 0.8 Ma, this fluvial source of material was less evident. In conjunction with this, productivity decreased and the main primary producer changed.

CONCLUSIONS

Two areas of study, Sites 1076 and 1077, located in the Congo Basin, and Site 1081, situated on the Walvis Ridge, were selected to reconstruct climate change over the past 1.5 m.y. off the western coast of Africa. A multiproxy approach was adopted, involving the use of various analyses and techniques to generate several proxy records. A synthesis of the overall evolution of the two regions is provided in Figures F5 and F6. In particular, there is evidence for the influence of the MPR, yet, in addition, the records demonstrate that the continent and the ocean continued to respond to change following this event, both on long and short timescales.

Furthermore, the records from these two areas demonstrate that despite their close proximity, much of the variability in the records is localized. In particular, proxy productivity records at the Walvis Ridge show clear interglacial–glacial cyclicity with enhanced values occurring during glacial periods, assumed to be a response to enhanced upwelling and possibly intensification of the Benguela Current (Durham, 2000).

Productivity in the Congo Basin is highly localized and, in fact, differs between the two sites, Holes 1076A and 1077A. These records show no clear glacial or interglacial cyclicity and instead are driven by a complex interaction of marine upwelling and influxes of nutrient-enriched waters from the Congo River.

In addition, the evidence from these records shows that there may not necessarily be a simple response to apparently simple or linear changes and that numerous factors may influence records from deep-sea sediments. It also demonstrates the complexity of the climate system, which responds on both long and short timescales, yet also appears to be dependent on the reaching of thresholds and the impacts of unpredicted and unpredictable events.

ACKNOWLEDGMENTS

REFERENCES

Berger, A., and Loutre, M.F., 1991. Insolation values for the climate of the last 10 million years. *Quat. Sci. Rev.,* 10:297–317.

Berger, W.H., and Wefer, G., 1996. Expeditions into the past: paleoceanographic studies in the South Atlantic. *In* Wefer, G., Berger, W.H., Siedler, G., Webb, D.J. (Eds.), *The South Atlantic: Present and Past Circulation:* Berlin (Springer-Verlag), 363–410.

Berger, W.H., Wefer, G., Richter, C., Lange, C.B., Giraudeau, J., Hermelin, O., and Shipboard Scientific Party, 1998a. The Angola-Benguela upwelling system: paleoceanographic synthesis of shipboard results from Leg 175. *In* Wefer, G., Berger, W.H., and Richter, C., et al., *Proc. ODP, Init. Repts.,* 175: College Station, TX (Ocean Drilling Program), 505–531.

Berger, W.H., Wefer, G., Richter, C., and Shipboard Scientific Party, 1998b. Color cycles in Quaternary sediments from the Congo Fan region (Site 1075): a statistical analysis. *In* Wefer, G., Berger, W.H., and Richter, C., et al., *Proc. ODP, Init. Repts.,* 175: College Station, TX (Ocean Drilling Program), 561–567.

Berggren, W.A., Kent, D.V., Swisher, C.C., III, and Aubry, M.-P., 1995. A revised Cenozoic geochronology and chronostratigraphy. *In* Berggren, W.A., Kent, D.V., Aubry, M.-P., and Hardenbol, J. (Eds.), *Geochronology, Time Scales and Global Stratigraphic Correlation.* Spec. Publ.—Soc. Econ. Paleontol. Mineral. (Soc. Sediment. Geol.), 54:129–212.

Brassell, S.C., Eglinton, G., Marlowe, I.T., Pflaumann, U., and Sarnthein, M., 1986. Molecular stratigraphy: a new tool for climatic assessment. *Nature,* 320:129–133.

Broecker, W.S., and van Donk, J., 1970. Insolation changes, ice volumes, and the O^{18} record in deep-sea cores. *Rev. Geophys. Space Phys.,* 8:169–198.

Dean, W., and Gardner, J., 1985. Cyclic variations in calcium carbonate and organic carbon in Miocene to Holocene sediments, Walvis Ridge, South Atlantic Ocean. *In* Hsü, K.J., and Weissert, H.J. (Eds.), *South Atlantic Paleoceanography:* Cambridge (Cambridge Univ. Press), 61–78.

Dean, W.E., and Parduhn, N.L., 1984. Inorganic geochemistry of sediments and rocks recovered from the southern Angola Basin and adjacent Walvis Ridge, Sites 530 and 532, Deep Sea Drilling Project Leg 75. *In* Hay, W.W., Sibuet, J.-C., et al., *Init. Repts. DSDP,* 75: Washington (U.S. Govt. Printing Office), 923–958.

deMenocal, P.B., Ruddiman, W.F., and Pokras, E.M., 1993. Influence of high- and low-latitude on African terrestrial climate: Pleistocene eolian records from equatorial Atlantic Ocean Drilling Program Site 663. *Paleoceanography,* 8:209–242.

Diekmann, B., Kuhn, G., MacKensen, A., Petschick, R., Fütterer, D.K., Gersonde, R., Rühlemann, C., and Niebler, H.-S., 1999. Kaolinite and chlorite as tracers of modern and late Quaternary deep water circulation in the South Atlantic and the adjoining Southern Ocean. *In* Fischer, G., and Wefer, G. (Eds.), *Proxies in Paleoceanography: Examples from the South Atlantic:* Heidelberg (Springer), 285–313.

Diester-Haass, L., 1985. Late Quaternary upwelling history off southwest Africa (DSDP Leg 75, HPC 532). *In* Hsü, K.J., and Weissert, H.J. (Eds.), *South Atlantic Paleoceanography:* Cambridge (Cambridge Univ. Press), 47–55.

Diester-Haass, L., Heine, K., Rothe, P., and Schrader, H., 1988. Late Quaternary history of continental climate and the Benguela Current off South West Africa. *Palaeogeogr., Palaeoclimatol., Palaeoecol.,* 65:81–91.

Diester-Haass, L., Meyers, P.A., and Rothe, P., 1992. The Benguela Current and associated upwelling on the southwest African margin: a synthesis of the Neogene-Quaternary sedimentary record at DSDP Sites 362 and 352. *In* Summerhayes, C.P., Prell, W.L., and Emeis, K.C. (Eds.), *Upwelling Systems: Evolution Since the Early Miocene.* Geol. Soc. Spec. Publ. London, 64:331–342.

Diester-Haass, L., and Rothe, P., 1987. Plio–Pleistocene sedimentation on the Walvis Ridge, SE Atlantic (DSDP Leg 75, Site 532): influence of surface currents, carbonate dissolution and climate. *Mar. Geol.,* 77:53–85.

Dupont, L.M., Beug, H.-J., Stalling, H., and Tiedemann, R., 1989. First palynological results from Site 658 at 21°N off Northwest Africa: pollen as climate indicators. *In* Ruddiman, W., Sarnthein, M., et al., *Proc. ODP, Sci. Results,* 108: College Station, TX (Ocean Drilling Program), 93–111.

Durham, E.L., 2000. Reconstructing the climatic history of the western coast of Africa over the past 1.5 million years. A comparison of proxy records from the Congo Basin and the Walvis Ridge [Ph.D. dissert.] Univ. London, United Kingdom.

Emeis, K.-C., Doose, H., Mix, A., and Schulz-Bull, D., 1995. Alkenone sea-surface temperatures and carbon burial at Site 846 (eastern equatorial Pacific Ocean): the last 1.3 m.y. *In* Pisias, N.G., Mayer, L.A., Janecek, T.R., Palmer-Julson, A., and van Andel, T.H. (Eds.), *Proc. ODP, Sci. Results,* 138: College Station, TX (Ocean Drilling Program), 605–613.

Frederichs, T., Bleil, U., Däumler, K., von Dobeneck, T., and Schmidt, A.M., 1999. The magnetic view on the marine paleoenvironment: parameters, techniques, and potentials of rock magnetic studies as a key to paleoclimatic and paleoceanographic changes. *In* Fischer, G., and Wefer, G. (Eds.), *Use of Proxies in Paleoceanography: Examples from the South Atlantic:* Berlin (Springer-Verlag), 575–599.

Haq, B.U., Hardenbol, J., and Vail, P.R., 1987. Chronology of fluctuating sea levels since the Triassic. *Science,* 235:1156–1167.

Harris, P.G., Zhao, M., Rosell-Melé, A., Tiedemann, R., Sarnthein, M., and Maxwell, J.R., 1996. Chlorine accumulation rate as a proxy for Quaternary marine primary productivity. *Nature,* 383:63–65.

Hay, W.W., and Brock, J.C., 1992. Temporal variation in intensity of upwelling off southwest Africa. *In* Summerhayes, C.P., Prell, W.L., and Emeis, K.C. (Eds.), *Upwelling Systems: Evolution Since the Early Miocene.* Geol. Soc. Spec. Publ. London, 64:463–497.

Imbrie, J., Berger, A., Boyle, E., Clemens, S., Duffy, A., Howard, W., Kukla, G., Kutzbach, J., Martinson, D., McIntyre, A., Mix, A., Molfino, B., Morley, J., Peterson, L., Pisias, N., Prell, W., Raymo, M., Shackleton, N., and Toggweiler, J., 1993. On the structure and origin of major glaciation cycles, 2. The 100,000-year cycle. *Paleoceanography,* 8:699–735.

Imbrie, J., Boyle, E.A., Clemens, S.C., Duffy, A., Howard, W.R., Kukla, G., Kutzbach, J., Martinson, D.G., McIntyre, A., Mix, A.C., Molfino, B., Morley, J.J., Peterson, L.C., Pisias, N.G., Prell, W.L., Raymo, M.E., Shackleton, N.J., and Toggweiler, J.R., 1992. On the structure and origin of major glaciation cycles, 1. Linear responses to Milankovitch forcing. *Paleoceanography,* 7:701–738.

Imbrie, J., Hays, J.D., Martinson, D.G., McIntyre, A., Mix, A.C., Morley, J.J., Pisias, N.G., Prell, W.L., and Shackleton, N.J., 1984. The orbital theory of Pleistocene climate: support from a revised chronology of the marine [0100S]^{18}O record. *In* Berger, A., Imbrie, J., Hays, J., Kukla, G., and Saltzman, B. (Eds.), *Milankovitch and Climate* (Pt. 1), NATO ASI Ser. C, Math Phys. Sci., 126:269–305.

Jansen, J.H.F., Ufkes, E., and Schneider, R.R., 1996. Late Quaternary movements of the Angola-Benguela-Front, SE Atlantic, and implications for advection in the equatorial ocean. *In* Wefer, G., Berger, W.H., Siedler, G., and Webb, D. (Eds.), *The South Atlantic: Present and Past Circulation:* Berlin (Springer-Verlag), 553–575.

Jansen, J.H.F., and van Iperen, J.M., 1991. A 220,000-year climatic record for the east equatorial Atlantic Ocean and equatorial Africa: evidence from diatoms and opal phytoliths in the Zaire (Congo) deep-sea fan. *Paleoceanography,* 6:573–591.

Jansen, J.H.F., van Weering, T.C.E., Gieles, R., and van Iperen, J., 1984. Middle and late Quaternary oceanography and climatology of the Zaire-Congo fan and the adjacent eastern Angola Basin. *Neth. J. Sea Res.,* 17:201–249.

Kent, D.V., 1982. Apparent correlation of paleomagnetic intensity and climatic records in deep-sea sediments. *Nature,* 299:538–539.

Little, M.G., Schneider, R.R., Kroon, D., Price, B., Bickert, T., and Wefer, G., 1997. Rapid paleoceanographic changes in the Benguela Upwelling System for the last

160,000 years as indicated by abundances of planktonic foraminifera. *Palaeogeogr., Palaeoclimatol., Palaeoecol.,* 130:135–161.

Martin, J.H., 1992. Iron as a limiting factor in ocean productivity. *In* Falkowski, P., Woodhead, A.D., and Vivirito, K. (Eds.), *Primary Productivity and Biogeochemical Cycles in the Sea:* New York (Plenum Press), 123–137.

McIntyre, A., Kipp, N.G., Bé, A.W.H., Crowley, T., Kellogg, T., Gardner, J.V., Prell, W., and Ruddiman, W.F., 1976. The glacial North Atlantic 18,000 years ago: a CLIMAP reconstruction. *In* Cline, R.M., and Hays, J.D. (Eds.), *Investigation of Late Quaternary Paleoceanography and Paleoclimatology.* Mem. Geol. Soc. Am., 145:43–76.

McIntyre, A., Ruddiman, W.F., Karlin, K., and Mix, A.C., 1989. Surface water response of the equatorial Atlantic Ocean to orbital forcing. *Paleoceanography,* 4:19–55.

Meeuwis, J.M., and Lutjeharms, J.R.E., 1990. Surface thermal characteristics of the Angola-Benguela Front. *S. Afr. J. Mar. Sci.,* 9:261–279.

Meyers, P.A., 1997. Organic geochemical proxies of paleoceanographic, paleolimnologic, and paleoclimatic processes. *Org. Geochem.,* 27:213–250.

Milankovitch, M., 1930. *Mathematische Klimalehre und Astronomische Theorie der Klimaschwankungen:* Berlin (Gebruder Borntaeger).

Oberhänsli, H., 1991. Upwelling signals at the northeastern Walvis Ridge during the past 500,000 years. *Paleoceanography,* 6:53–71.

Pastouret, L., Chamley, H., Delibrias, G., Duplessy, J.-C., and Thiede, J., 1978. Late Quaternary climatic changes in western tropical Africa deduced from deep-sea sedimentation off the Niger delta. O*ceanol. Acta,* 1:217–232.

Peterson, R.G., and Stramma, L., 1991. Upper-level circulation in the South Atlantic Ocean. *Progr. Oceanogr.,* 26:1–73.

Prahl, F.G., Muehlhausen, L.A., and Zahnle, D.L., 1988. Further evaluation of long-chain alkenones as indicators of paleoceanographic conditions. *Geochim. Cosmochim. Acta,* 52:2303–2310.

Prahl, F.G., and Wakeham, S.G., 1987. Calibration of unsaturation patterns in long-chain ketone compositions for paleotemperature assessment. *Nature,* 330:367–369.

Prell, W.L., 1982. Oxygen and carbon isotope stratigraphy for the Quaternary of Hole 502B: evidence for two modes of isotopic variability. *In* Prell, W.L., Gardner, J.V., et al., *Init. Repts. DSDP,* 68: Washington (U.S. Govt. Printing Office), 455–464.

Raymo, M.E., Ruddiman, W.F., Shackleton, N.J., and Oppo, D.W., 1990. Evolution of Atlantic-Pacific $\delta^{13}C$ gradients over the last 2.5 m.y. *Earth Planet. Sci. Lett.,* 97:353–368.

Reid, J.R., 1996. On the circulation of the South Atlantic Ocean. *In* Wefer, G., Berger, W.H., Siedler, G., and Webb, D.J. (Eds.), *The South Atlantic: Present and Past Circulation:* Berlin (Springer-Verlag), 13–44.

Rosell-Melè, A., Carter, J., and Eglinton, G., 1994. Distribution of long-chain alkenones and alkyl alkenoates in marine surface sediments from the North East Atlantic. *In* Telnaes, N., van Graas, G., and Oygard, K. (Eds.), *Advances in Organic Geochemistry 1993: Proc. 16th Int. Meet. on Org. Geochem.* Org. Geochem., 22:501–509.

Rosell-Melé, A., Carter, J.F., Parry A.T., and Eglinton, G., 1995. Determination of the U^k_{37} index in geological samples. *Anal. Chem.,* 67:1283–1289.

Rosell-Melé, A., and Koç, N., 1997. Paleoclimatic significance of the stratigraphic occurrence of photosynthetic biomarker pigments in the Nordic seas. *Geology,* 25:49–52.

Ruddiman, W.F., Raymo, M.E., Martinson, D.G., Clement, B.M., and Backman, J., 1989. Pleistocene evolution: Northern Hemisphere ice sheets and North Atlantic Ocean. *Paleoceanography,* 4:353–412.

Schneider, R.R., Müller, P.J., and Ruhland, G., 1995. Late Quaternary surface circulation in the east equatorial South Atlantic: evidence from alkenone sea surface temperatures. *Paleoceanography*, 10:197–219.

Schneider, R.R., Price, B., Müller, P.J., Kroon, D., and Alexander, I., 1997. Monsoon-related variations in Zaire (Congo) sediment load and influence of fluvial silicate

supply on marine productivity in the east equatorial Atlantic during the last 200,000 years. *Paleoceanography,* 12:463–481.

Shackleton, N.J., Berger, A., and Peltier, W.A., 1990. An alternative astronomical calibration of the lower Pleistocene timescale based on ODP Site 677. *Trans. R. Soc. Edinburgh: Earth Sci.,* 81:251–261.

Shackleton, N.J., and Opdyke, N.D., 1977. Oxygen isotope and palaeomagnetic evidence for early Northern Hemisphere glaciation. *Nature,* 270:216–219.

Shannon, L.V., and Nelson, G., 1996. The Benguela: large scale features and processes and system variability. *In* Wefer, G., Berger, W.H., Siedler, G., Webb, D.J. (Eds.), *The South Atlantic: Present and Past Circulation:* Berlin (Springer-Verlag), 163–210.

Shipboard Scientific Party, 1998a. Introduction: background, scientific objectives, and principal results for Leg 175 (Benguela Current and Angola-Benguela upwelling systems). *In* Wefer, G., Berger, W.H., and Richter, C., et al., *Proc. ODP, Init. Repts.,* 175: College Station, TX (Ocean Drilling Program), 7–25.

————, 1998b. Explanatory notes. *In* Wefer, G., Berger, W.H., and Richter, C., et al., *Proc. ODP, Init. Repts.,* 175: College Station, TX (Ocean Drilling Program), 27–46.

————, 1998c. Site 1076. *In* Wefer, G., Berger, W.H., and Richter, C., et al., *Proc. ODP, Init. Repts.,* 175: College Station, TX (Ocean Drilling Program), 87–113.

————, 1998d. Site 1077. *In* Wefer, G., Berger, W.H., and Richter, C., et al., *Proc. ODP, Init. Repts.,* 175: College Station, TX (Ocean Drilling Program), 115–141.

————, 1998e. Site 1081. *In* Wefer, G., Berger, W.H., and Richter, C., et al., *Proc. ODP, Init. Repts.,* 175: College Station, TX (Ocean Drilling Program), 223–272.

Siesser, W.G., 1980. Late Miocene origin of the Benguela upwelling system off northern Namibia. *Science,* 208:283–285.

Singer, A., 1984. The paleoclimatic interpretation of clay minerals in sediments: a review. *Earth-Sci. Rev.,* 21:251–293.

Stein, R., ten Haven, H.L., Littke, R., Rullkötter, J., and Welte, D.H., 1989. Accumulation of marine and terrigenous organic carbon at upwelling Site 658 and nonupwelling Sites 657 and 659: implications for the reconstruction of paleoenvironments in the eastern subtropical Atlantic through late Cenozoic times. *In* Ruddiman, W., Sarnthein, M., et al., *Proc. ODP, Sci. Results,* 108: College Station, TX (Ocean Drilling Program), 361–385.

Summerhayes, C.P., Emeis, K.C., Angel, M.V., Smith, R.L., and Zeitschel, B., 1995. *Upwelling in the Ocean: Modern Processes and Ancient Records:* New York (Wiley and Sons), Dahlem Workshop Reports.

Thompson, R., and Oldfield, F., 1986. *Environmental Magnetism:* London (Allen and Unwin).

Tiedemann, R., Sarnthein, M., and Shackleton, N.J., 1994. Astronomic timescale for the Pliocene Atlantic $\delta^{18}O$ and dust flux records of Ocean Drilling Program Site 659. *Paleoceanography,* 9:619–638.

Tiedemann, R., Sarnthein, M., and Stein, R., 1989. Climatic changes in the western Sahara: aeolo-marine sediment record of the last 8 million years (Sites 657–661). *In* Ruddiman, W., Sarnthein, M., et al., *Proc. ODP, Sci. Results,* 108: College Station, TX (Ocean Drilling Program), 241–277.

Vail, P.R., Mitchum, R.M., Jr., and Thompson, S., III, 1977. Seismic stratigraphy and global changes of sea level, Part 3. Relative changes of sea level from coastal onlap. *In* Payton, C.E. (Ed.), *Seismic Stratigraphy: Applications to Hydrocarbon Exploration.* AAPG Mem., 26:63–81.

van Bennekom, A.J., and Berger, G.W., 1984. Hydrography and silica budget of the Angola Basin. *Neth. J. Sea Res.,* 17:149–200.

van Donk, J., 1976. ^{18}O record of the Atlantic Ocean for the entire Pleistocene Epoch. *In* Cline, R.M., and Hays, J.D. (Eds.), *Investigations of Late Quaternary Paleoceanography and Paleoclimatology.* Mem.—Geol. Soc. Am., 145:147–163.

Williams, M., Dunkerley, D., De Deckker, P., Kershaw, A.P., and Chappell, J., 1998. *Quaternary Environments* (2nd ed.): London (Arnold).

Figure F1. Location of Sites 1075–1087 drilled during ODP Leg 175. Sites 1076, 1077, and 1081, relevant to this study, are highlighted (from Shipboard Scientific Party, 1998a).
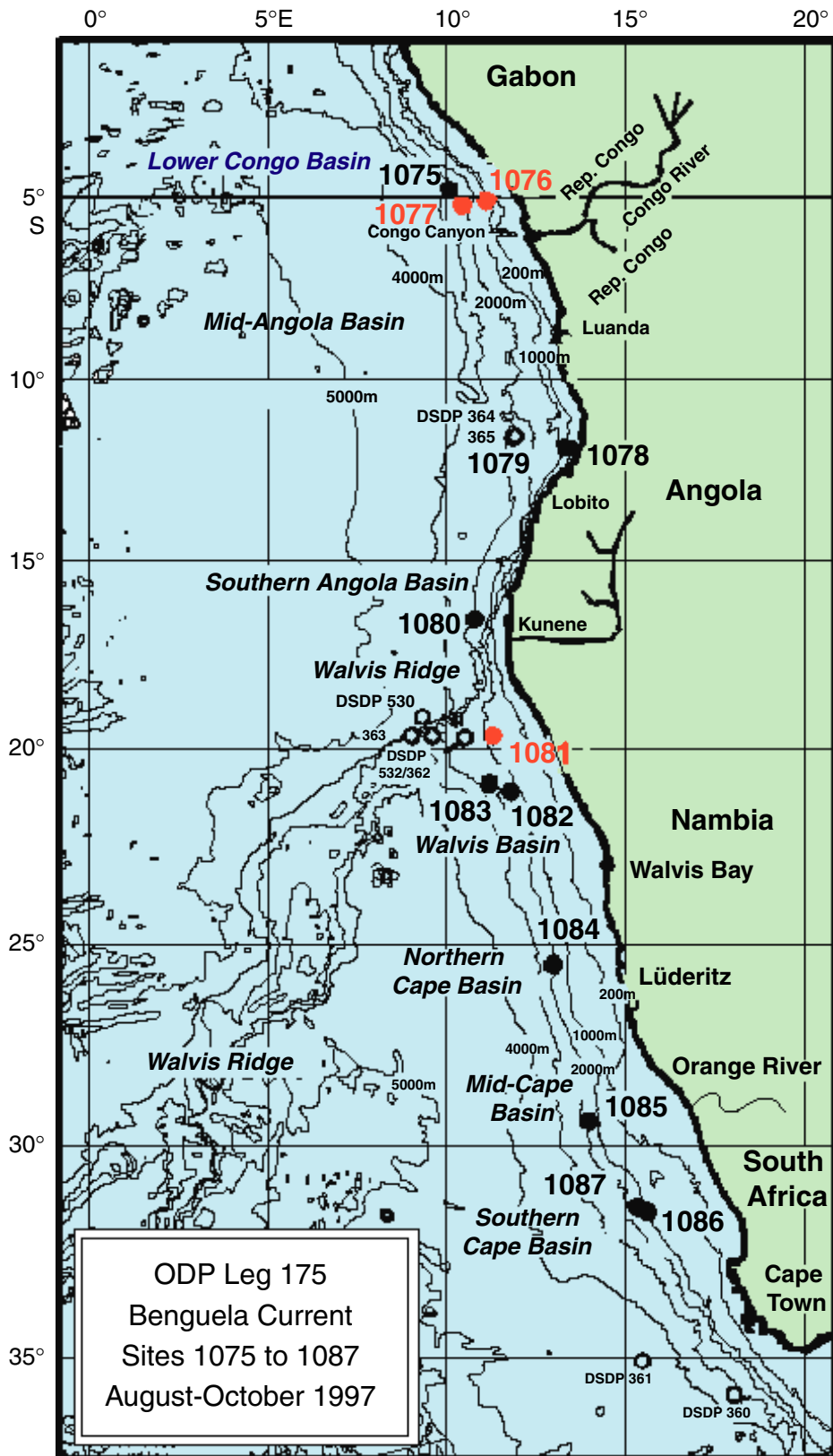
Figure F2. Large-scale oceanic circulation in the South Atlantic (from Shipboard Scientific Party, 1998a). ACC = Antarctic Circumpolar Current.
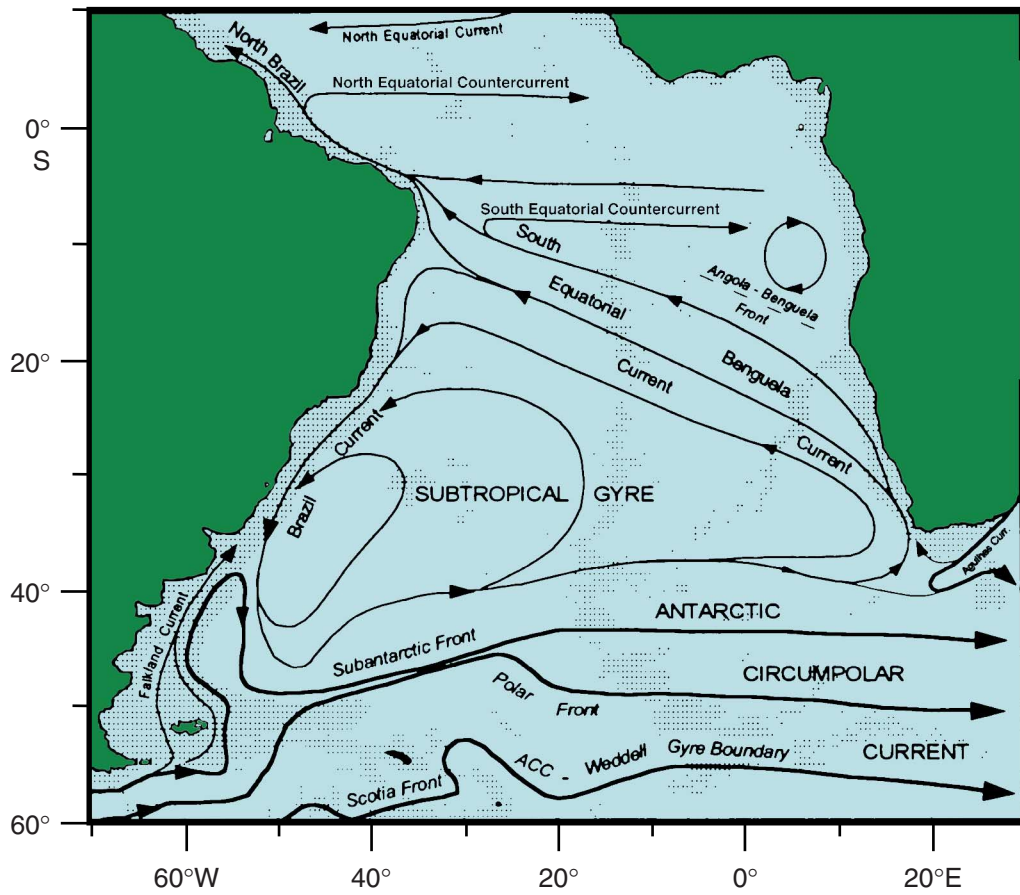
Figure F3. Schematic representation of the process for the extraction of organic matter based on the methodology of Rosell-Melé et al., 1995. DCM = dichloromethane, BST = bis(trimethyl)silyltrifluoroacetamide.
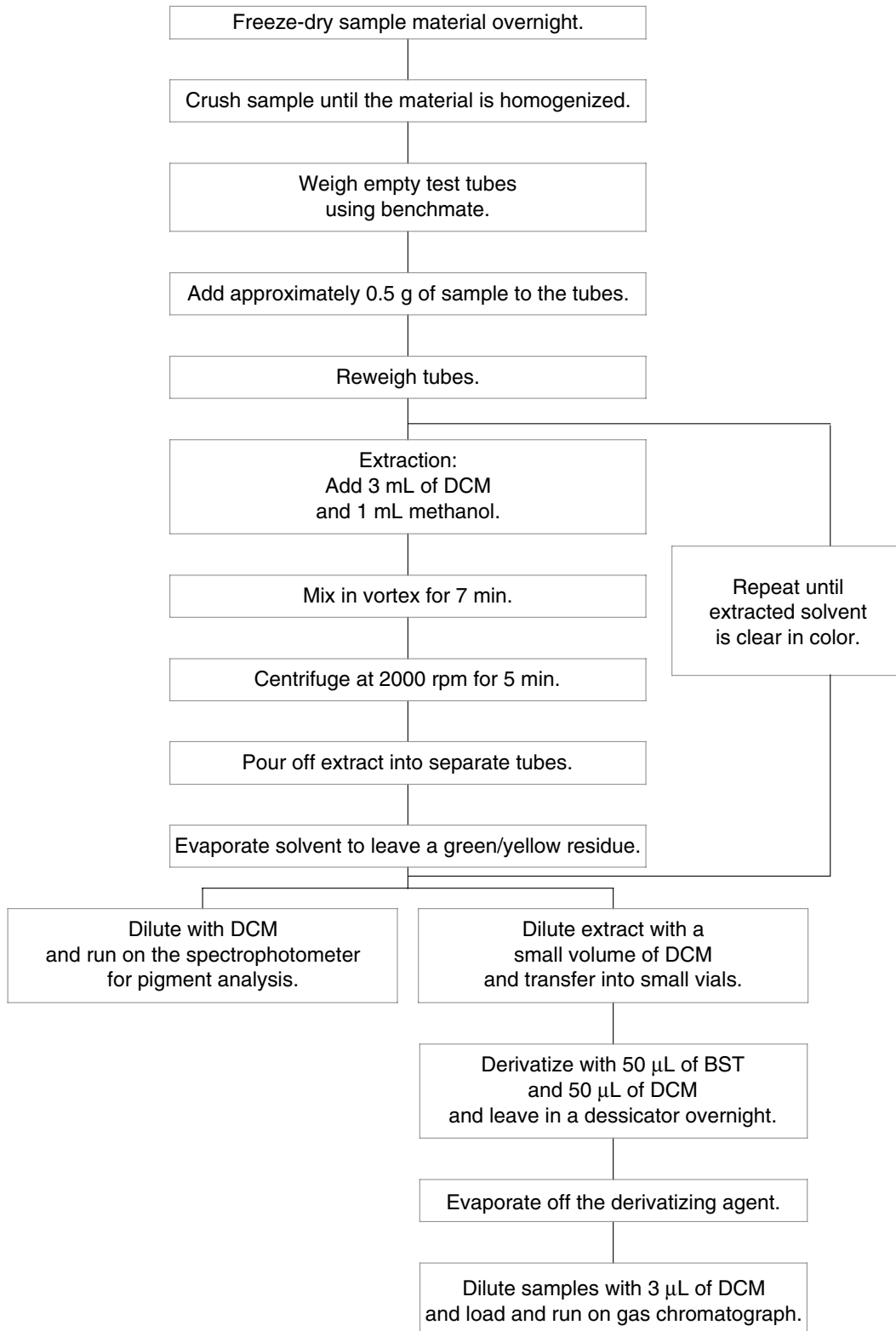
Figure F4. Age-depth plots for (**A**) Hole 1076A, (**B**) Hole 1077A, and (**C**) Hole 1081A.
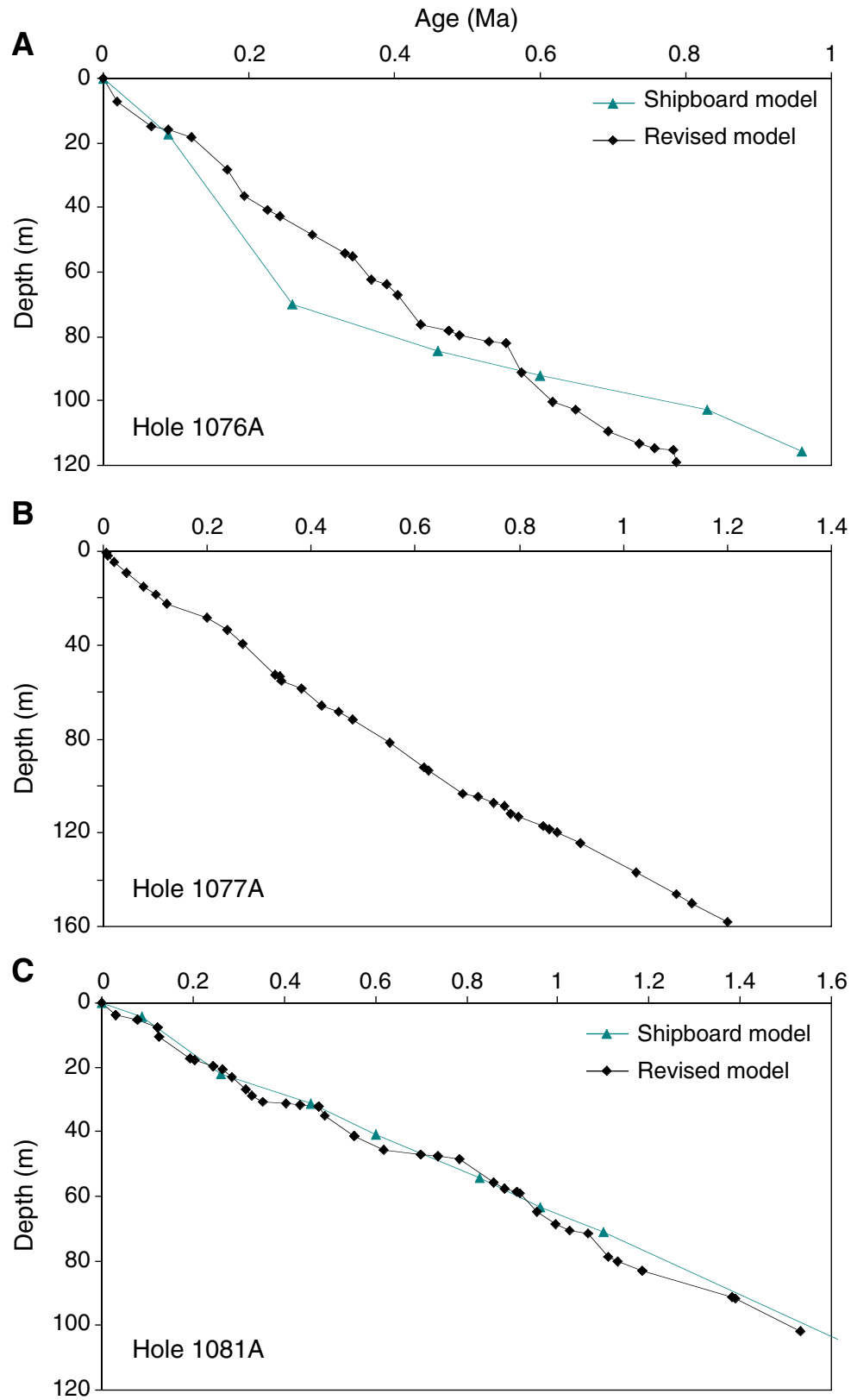
Figure F5. Schematic diagram of the overall transitions in fluvial terrigenous input, productivity (overall productivity and diatom abundance), and aridity established for Holes 1076A and 1077A, located in the Congo Basin, over the past 1.2 m.y. Periods of marine and terrigenous influences on productivity are shown, in addition to periods where incursions of waters from the south and north are identified. ABF = Angola-Benguela Front, MPR = mid-Pleistocene revolution.
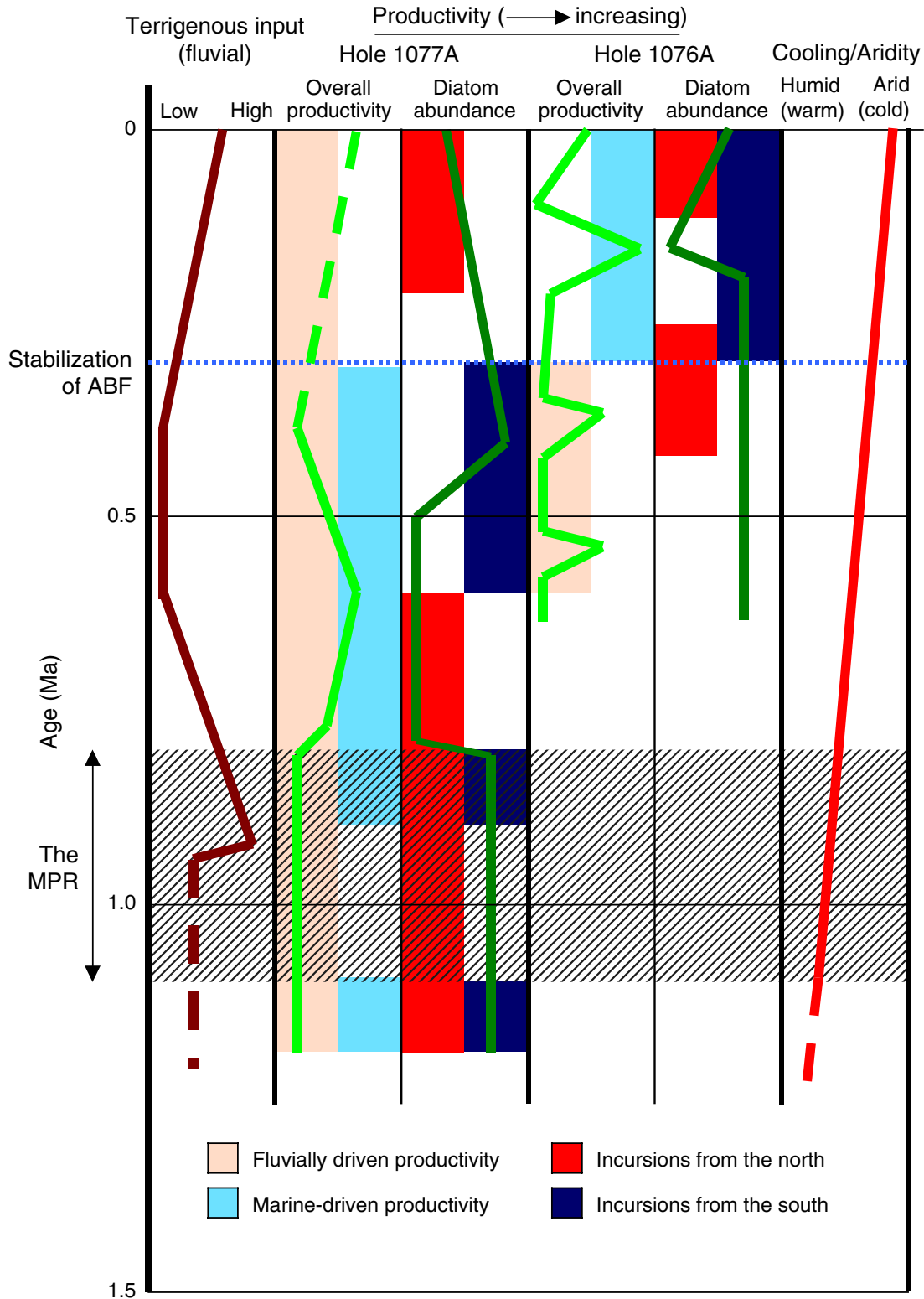
Figure F6. Schematic diagram of the overall transitions in terrigenous input (eolian and fluvial), productivity (overall productivity and diatom abundance), and sea level and aridity established for Hole 1081A, located on the Walvis Ridge, over the past 1.5 m.y. MPR = mid-Pleistocene revolution.
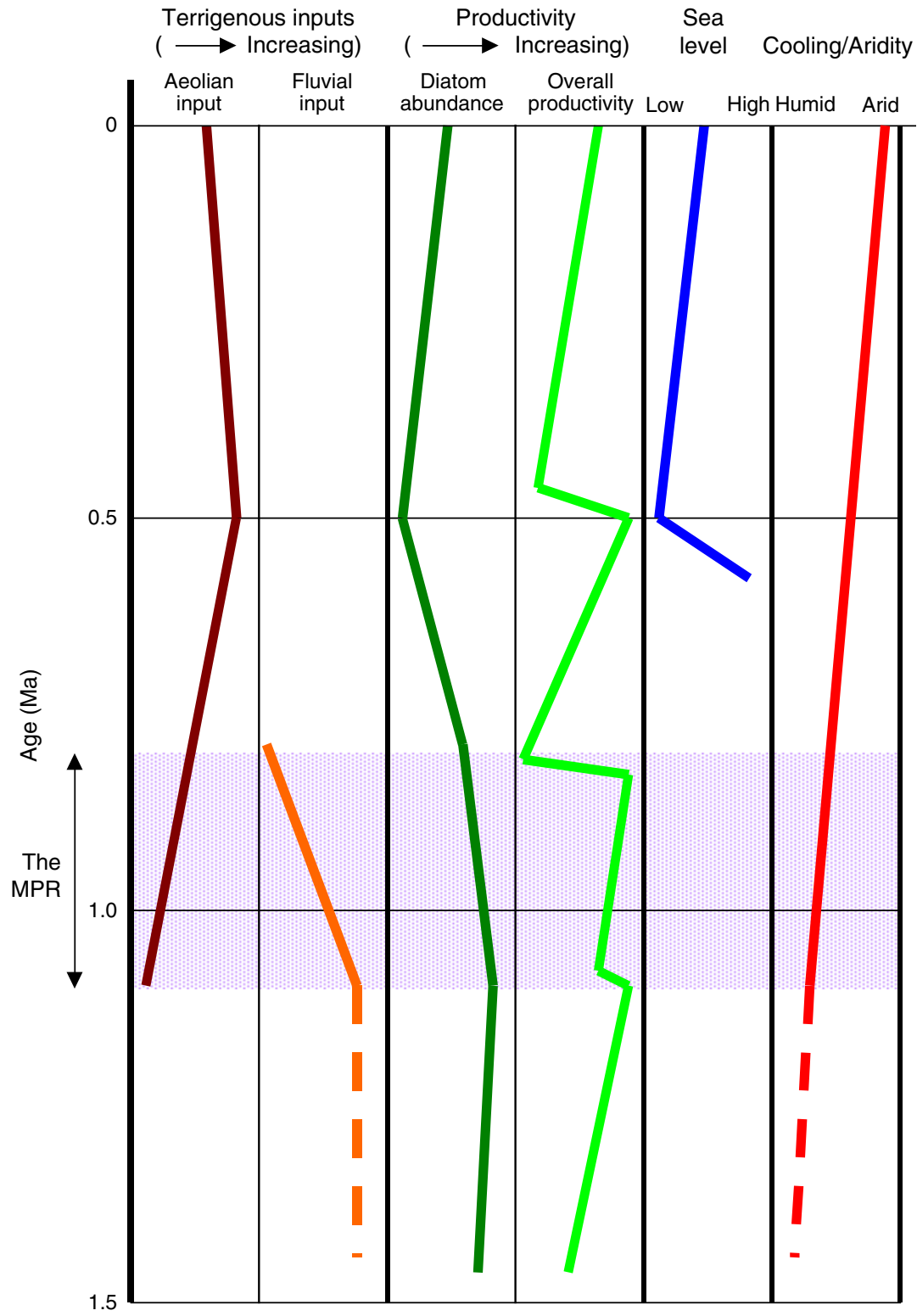
Figure F7. Records from Hole 1076A of (**A**) magnetic susceptibility, (**B**) shipboard magnetic susceptibility, (**C**) the δ^{18}O curve from *U. peregrina* vs. age, and (**D**) the standard δ^{18}O curve from Tiedemann et al. (1994). Isotope glacial Stages 2–18 from the SPECMAP timescale (Imbrie et al., 1984) are shaded.
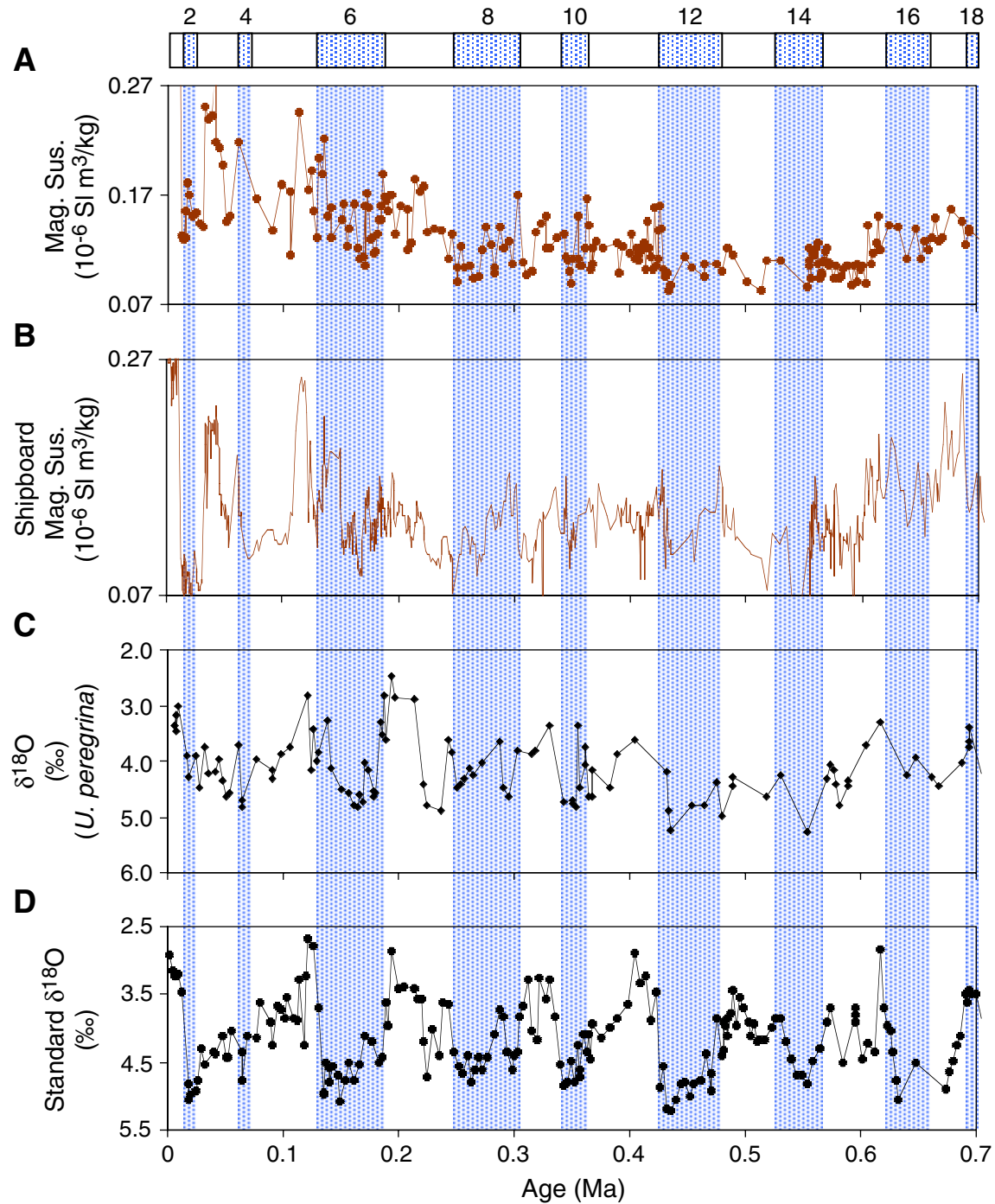
Figure F8. Records from Hole 1077A of (**A**) shipboard magnetic susceptibility, (**B**) magnetic susceptibility, and (**C**) the standard δ¹⁸O curve from Tiedemann et al. (1994). Glacial isotope Stages 2–50 from the SPEC-MAP timescale (2–22) (Imbrie et al., 1984) and Ruddiman et al., (1989) (22–50) are shaded.
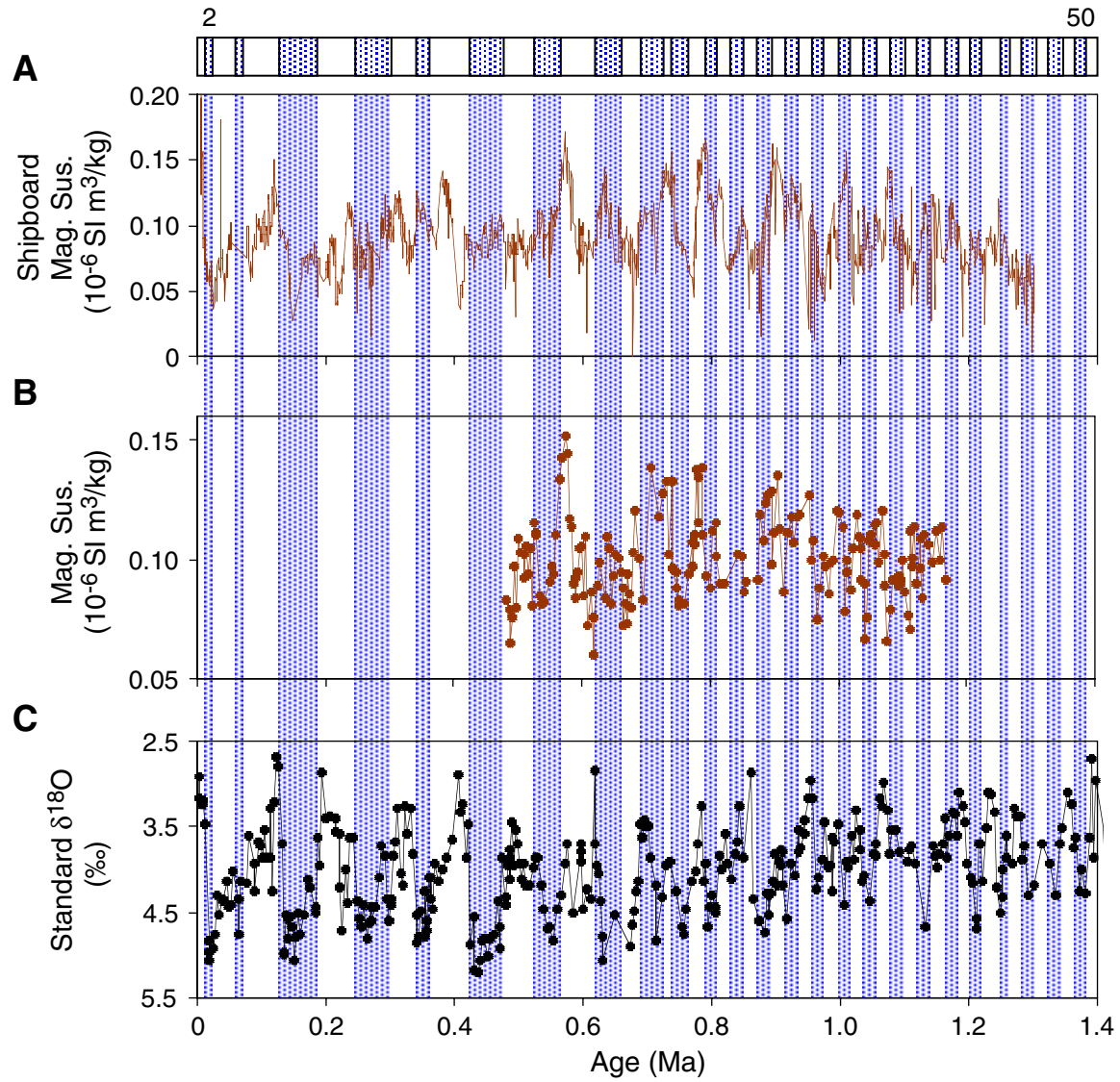
Figure F9. Records from Hole 1077A of (**A**) the 410/665 ratio and (**B**) magnetic susceptibility vs. age and (**C**) the 410/665 and (**D**) magnetic susceptibility records over the 0.5- to 0.7-Ma interval (shaded on A and B), plus (**E**) a scatter plot of the 410/665 ratio against magnetic susceptibility (10^{-6} SI m^3/kg).
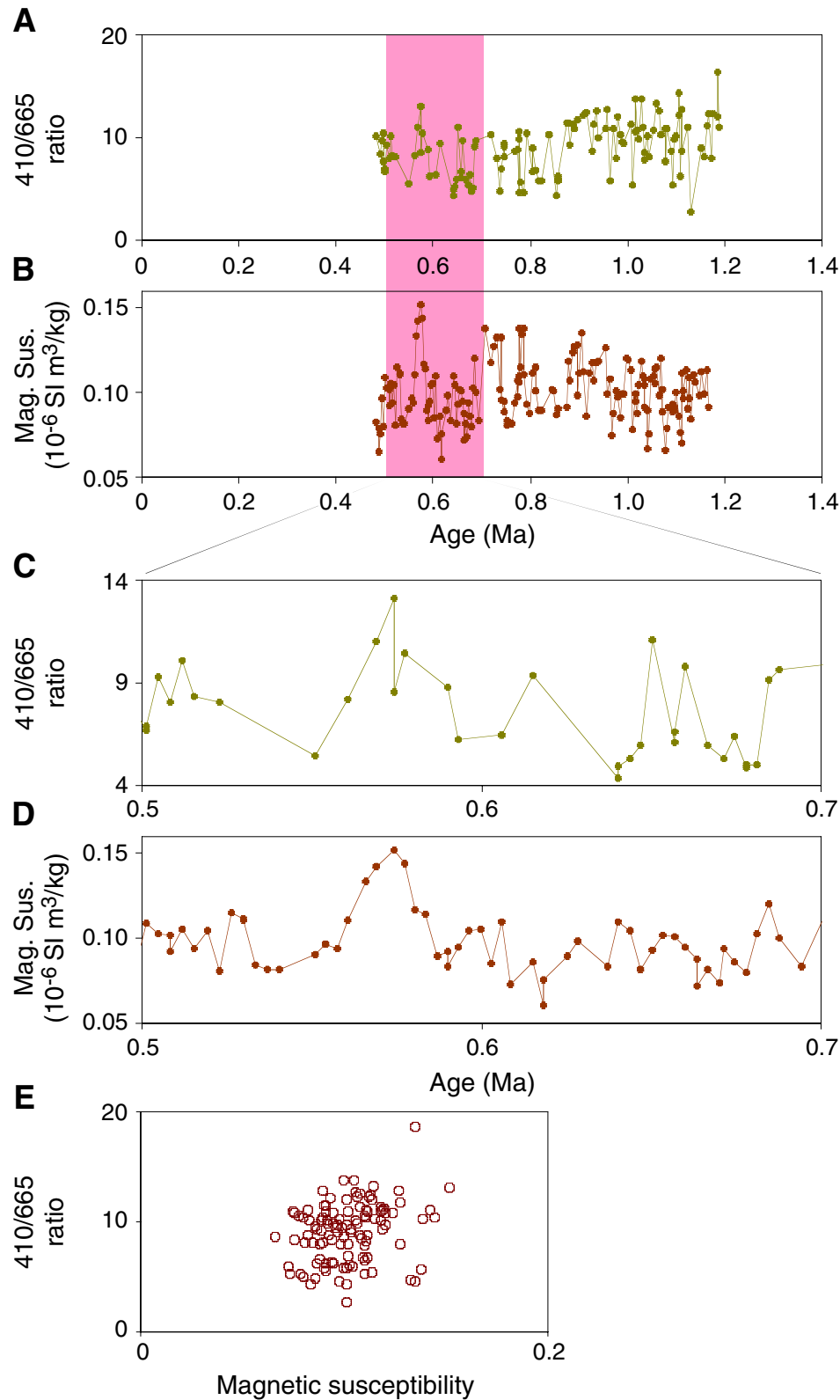
Figure F10. Comparison of (**A**) quartz concentrations and (**B**) kaolinite/(kaolinite+smectite) (k/[k+sm]) values from Hole 1076A with (**C**) quartz concentrations and (**D**) kaolinite/(kaolinite+smectite) values from Hole 1077A over the past 1.4 m.y. Glacial isotope Stages 2–50 from the SPECMAP timescale (2–22) (Imbrie et al., 1984) and Ruddiman et al., (1989) (22–50) are shaded.
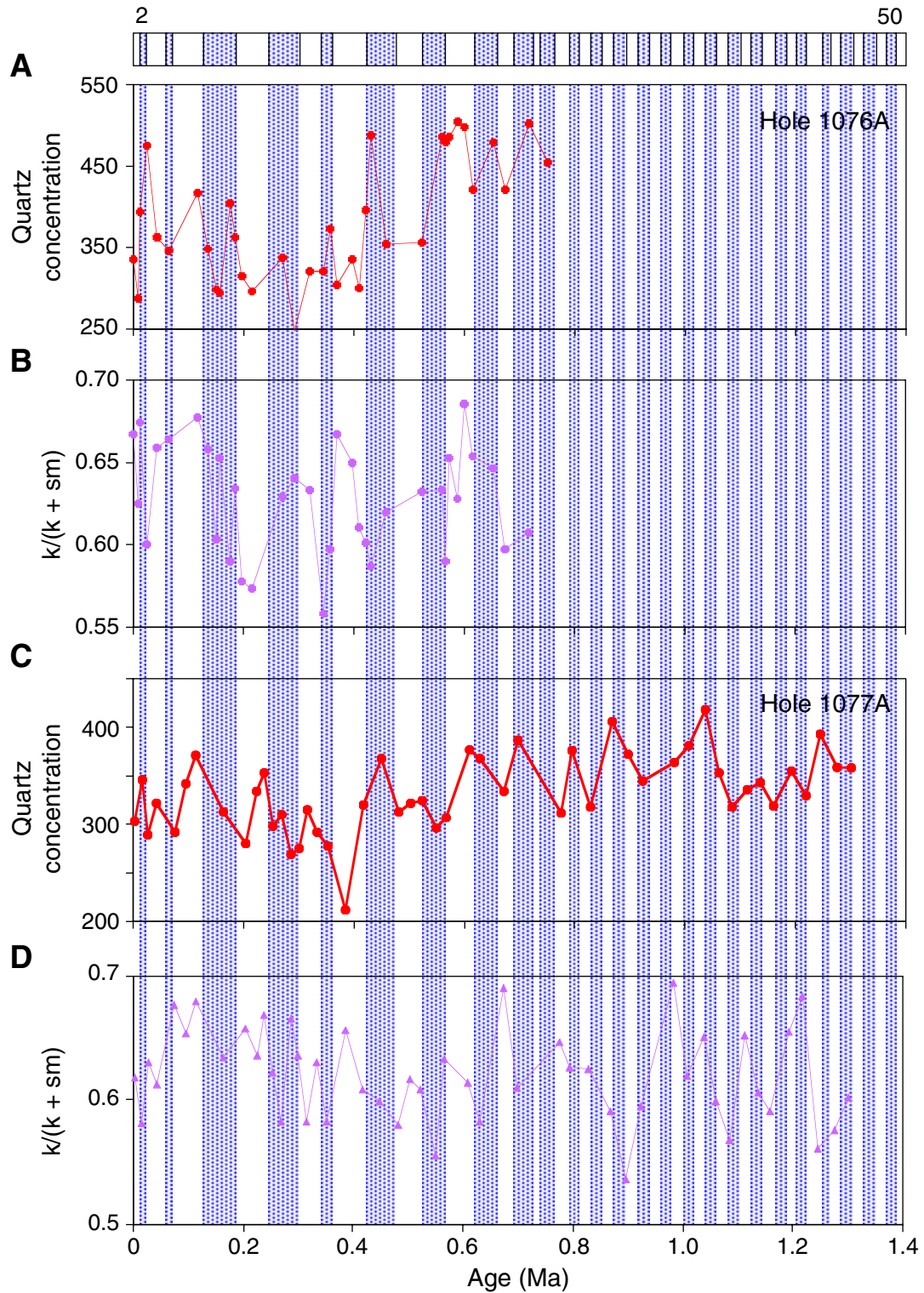
Figure F11. Records from Hole 1081A of (**A**) magnetic susceptibility, (**B**) shipboard magnetic susceptibility, (**C**) the δ^{18}O curve from *U. peregrina,* and (**D**) SST estimates vs. age and (**E**) the standard δ^{18}O curve from Tiedemann et al., (1994). Glacial Stages 2–56, from the SPECMAP timescale (2–22) (Imbrie et al., 1984) and Ruddiman et al., (1989) (22–56) are shaded. (**Figure shown on next page.**)

Figure F11 (continued). (Caption shown on previous page.).
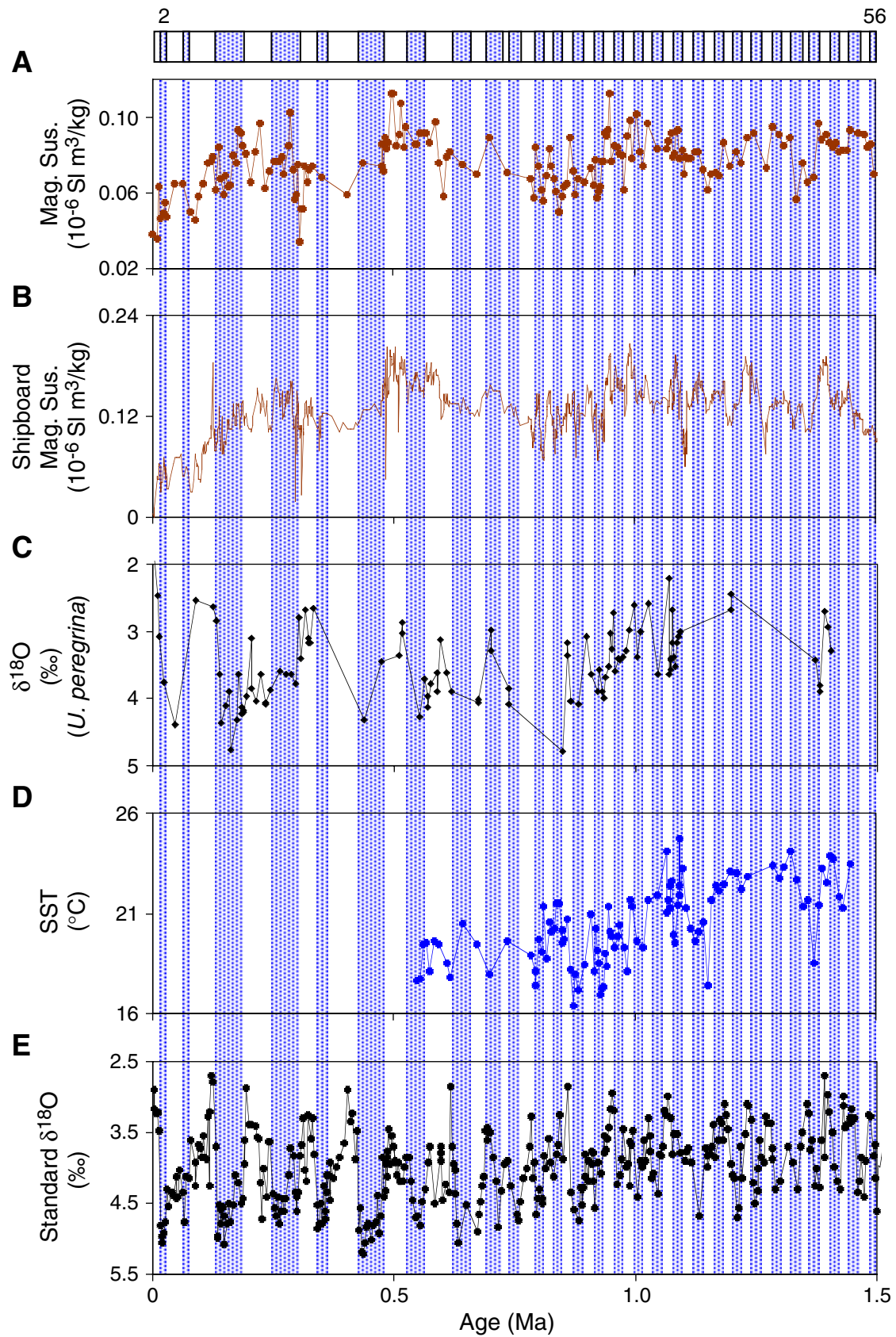
Figure F12. Records from Hole 1081A of (**A**) quartz concentrations, (**B**) the kaolinite/(kaolinite + smectite) (k/[k + s]) ratio, (**C**) kaolinite concentrations, (**D**) smectite concentrations, and (**E**) magnetic susceptibility vs. age. Glacial isotope Stages 2–56 from the SPECMAP timescale (2–22) (Imbrie et al., 1984) and Ruddiman et al., (1989) (22–56) are shaded.
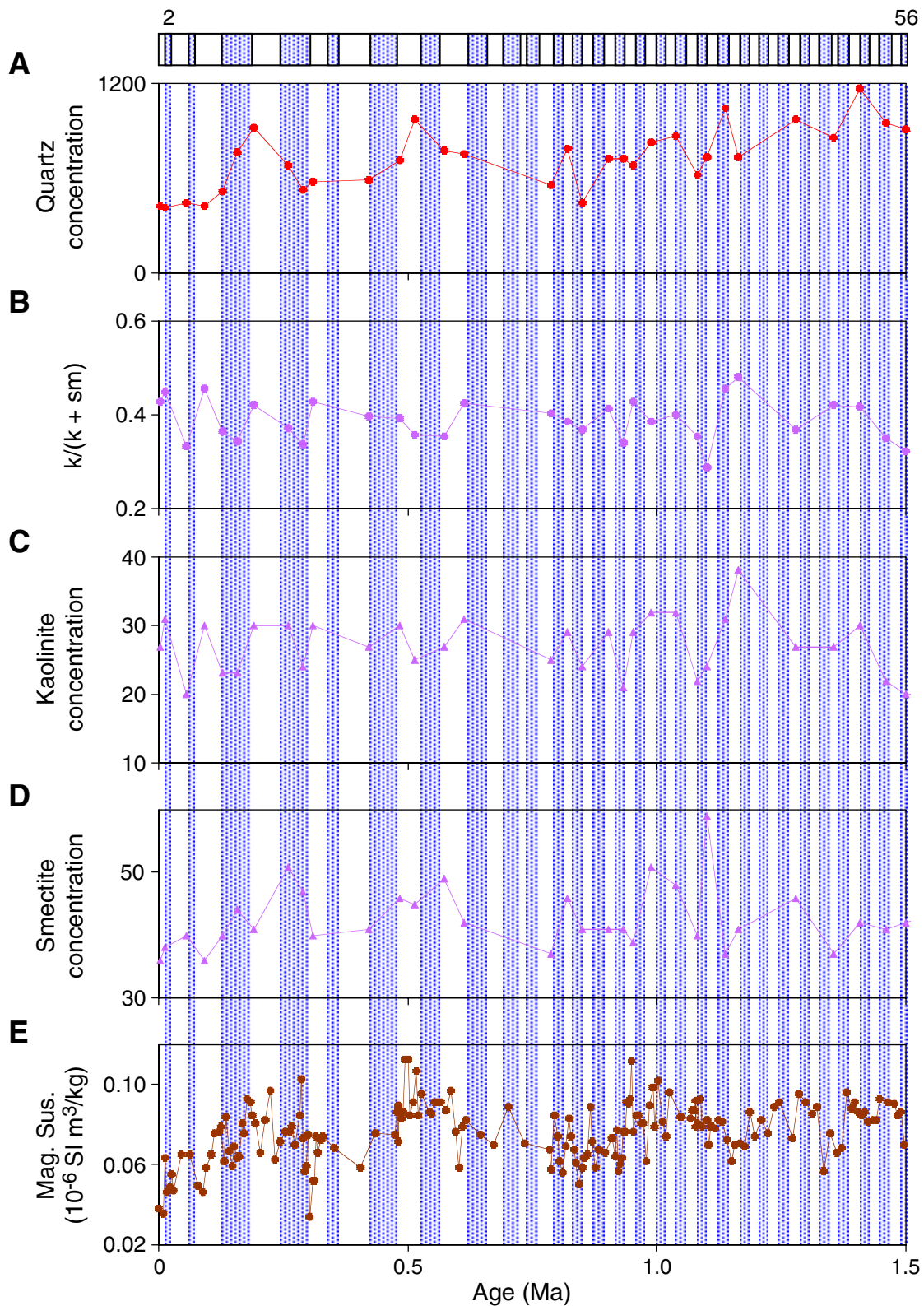
Figure F13. Scatter plots of chlorin mass accumulation rate (MAR) vs. chlorin concentration in (**A**) Hole 1076A, (**B**) Hole 1077A, and (**C**) Hole 1081A.
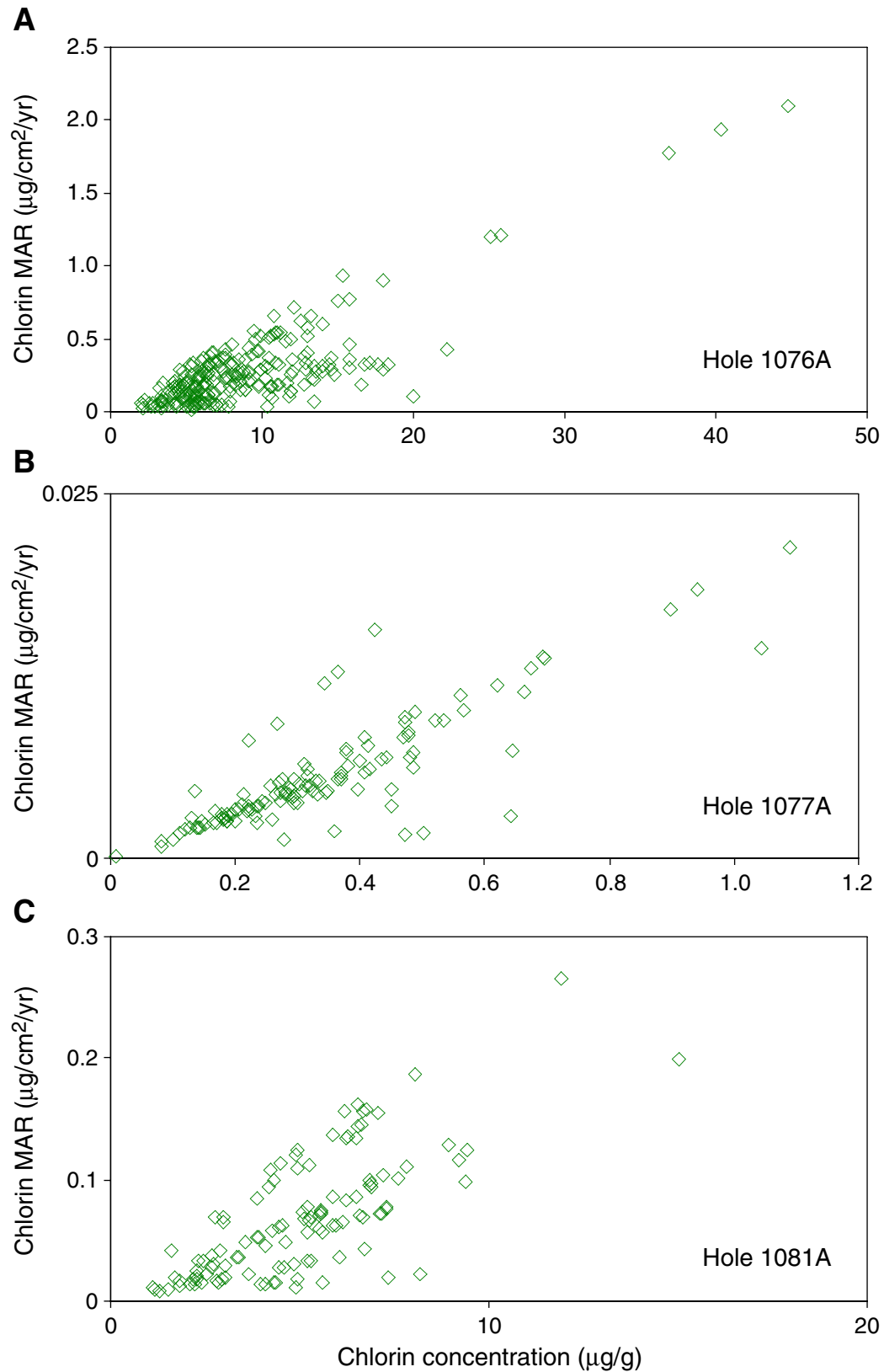
Figure F14. Records from Hole 1076A of (**A**) chlorin MAR, (**B**) TOC MAR, and (**C**) magnetic susceptibility vs. age. Glacial isotope Stages 2–18 from the SPECMAP timescale (Imbrie et al., 1984) are shaded. TOC = total organic carbon.
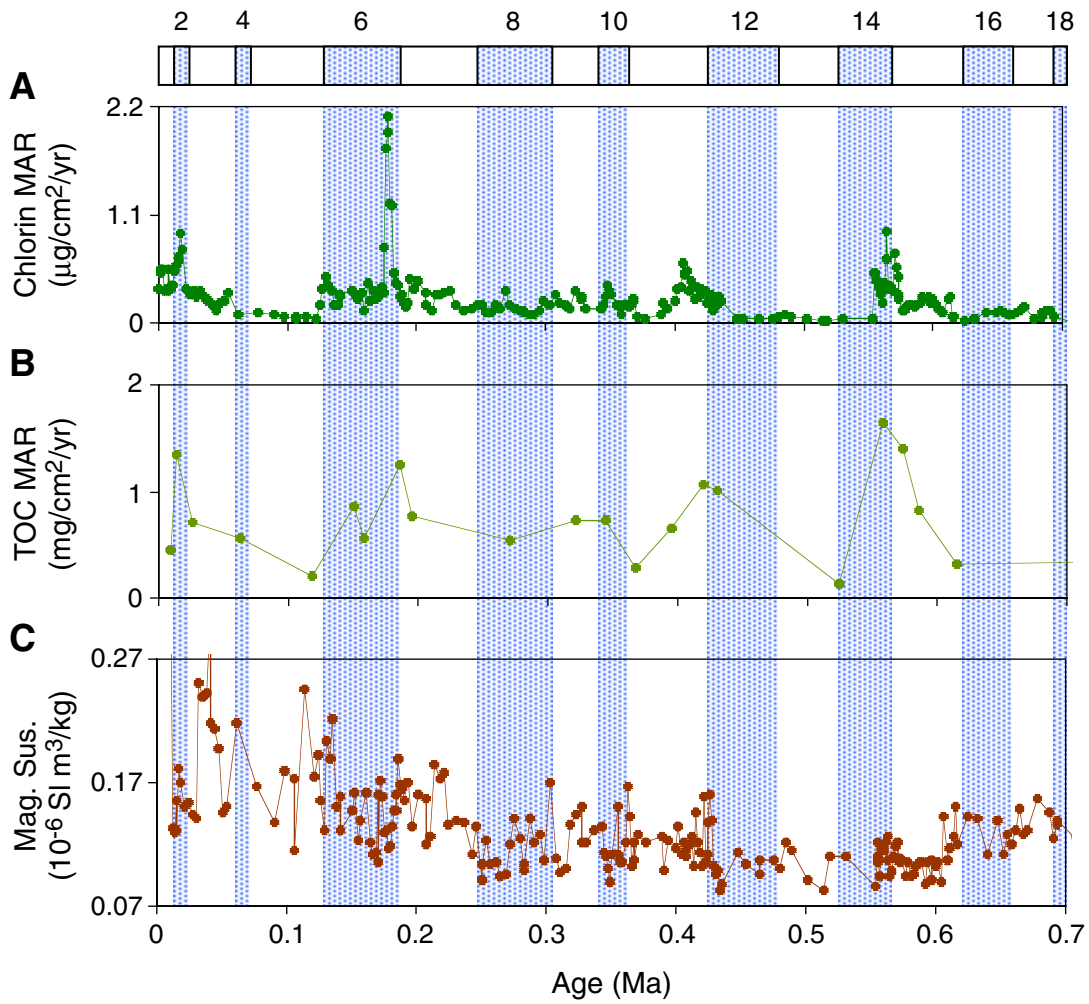
Figure F15. Records from Hole 1077A of (**A**) chlorin MAR, (**B**) TOC MAR, (**C**) shipboard TOC MAR, (**D**) sea-surface temperature (SST), and (**E**) magnetic susceptibility vs. age. Glacial isotope Stages 2–50 from the SPECMAP timescale (2–22) (Imbrie et al., 1984) and Ruddiman et al., (1989) (22–50) are shaded. MAR = mass accumulation rate, TOC = total organic carbon.
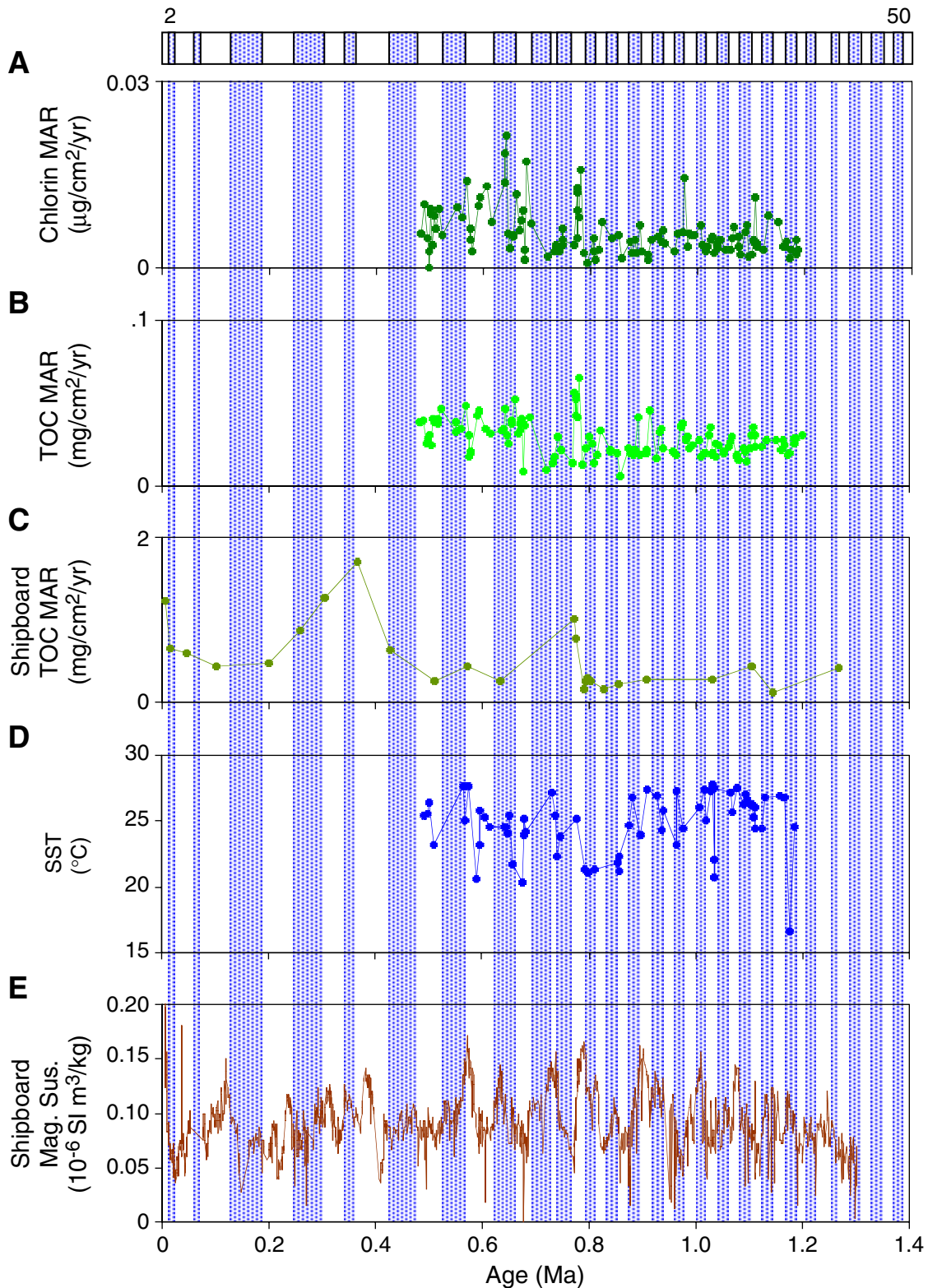
Figure F16. Records from Hole 1081A of (**A**) chlorin MAR, (**B**) TOC MAR, (**C**) shipboard TOC MAR, (**D**) sea-surface temperature (SST), and (**E**) magnetic susceptibility vs. age. Glacial isotope Stages 2–56 from the SPECMAP timescale (2–22) (Imbrie et al., 1984) and Ruddiman et al., (1989) (22–56) are shaded. MAR = mass accumulation rate, TOC = total organic carbon.
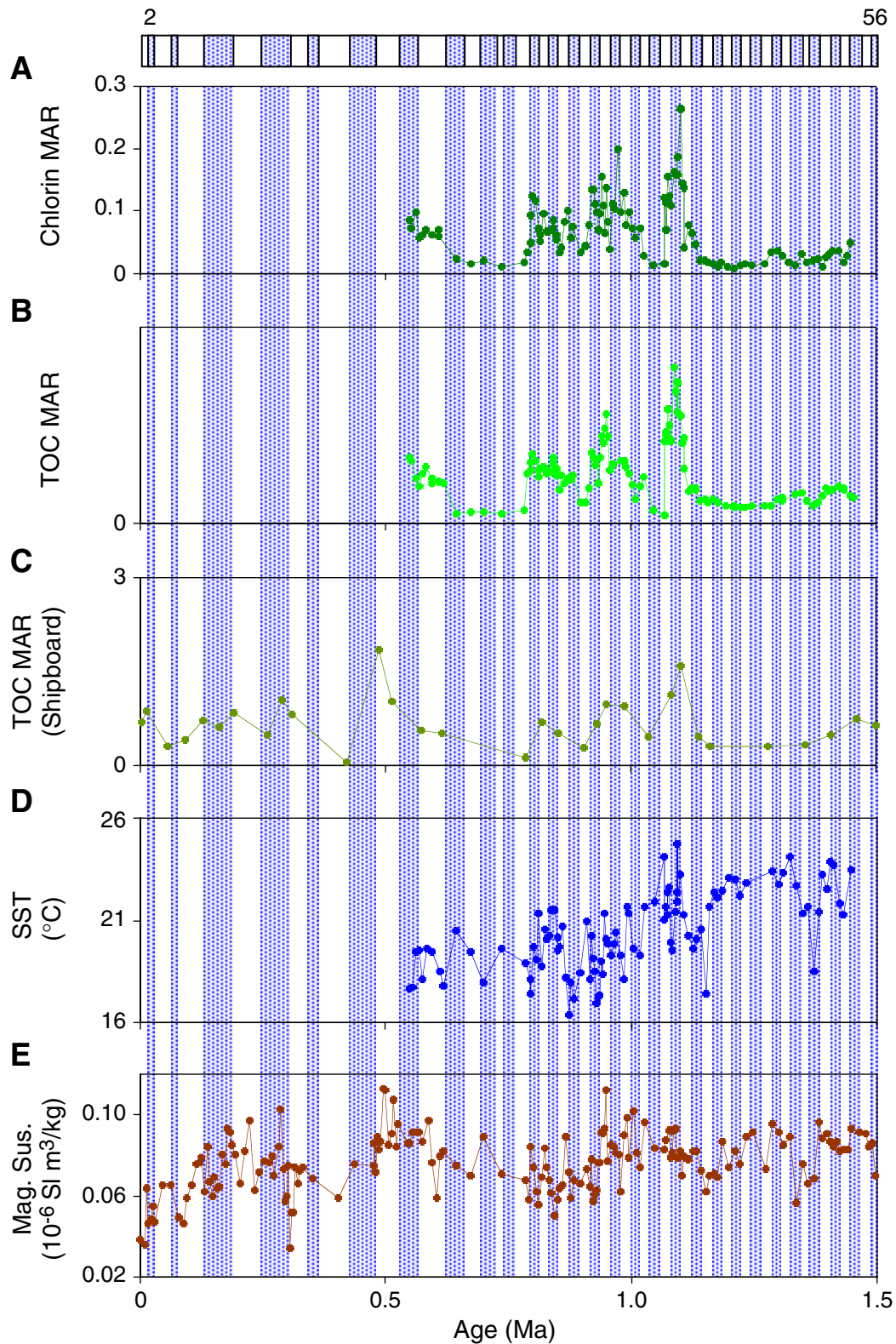
Table T1. Age-depth data based on δ¹⁸O data from the benthic foraminifer species *U. peregrina,* Hole 1076A.

Depth (m)	Age (Ma)
7.00	0.0183
15.00	0.0652
16.00	0.0901
18.00	0.1222
28.50	0.1710
36.50	0.1940
41.00	0.2249
42.50	0.2430
48.50	0.2870
54.00	0.3310
55.00	0.3425
62.23	0.3680
64.00	0.3887
67.00	0.4050
76.52	0.4360
78.32	0.4753
79.82	0.4898
81.50	0.5303
82.00	0.5537
91.00	0.5740
100.50	0.6170
102.50	0.6484
109.50	0.6940
113.40	0.7360
114.90	0.7570
115.40	0.7840

Table T2. Age-depth data based on shipboard bio-stratigraphic horizons, Hole 1076A.

Depth (m)	Age (Ma)
17.3	0.09
70.0	0.26
84.3	0.46
92.2	0.60
102.9	0.83
115.8	0.96

Note: Shipboard biostratigraphic horizons from Shipboard Scientific Party, 1998c.

Table T3. Age-depth data based on oxygen isotope
stratigraphy, Hole 1077A.

Depth (m)	Age (Ma)
0.85	0.006
1.75	0.008
4.55	0.022
9.25	0.046
15.42	0.078
18.59	0.100
22.39	0.122
28.29	0.200
33.89	0.237
39.69	0.268
52.77	0.331
53.57	0.339
55.07	0.343
58.45	0.382
65.98	0.420
68.75	0.453
71.95	0.481
81.63	0.550
92.13	0.617
93.43	0.626
103.13	0.690
104.43	0.722
107.15	0.750
108.47	0.771
112.07	0.784
113.17	0.798
117.47	0.846
118.77	0.857
119.67	0.872
124.57	0.917
137.07	1.026
146.35	1.101
150.45	1.132
158.15	1.199

Note: Oxygen isotope stratigraphy is from L.M. Dupont et al.,
(unpubl. data).

Table T4. Age-depth data based on $\delta^{18}O$ records, Hole 1081A.

Depth (m)	Age (Ma)
3.7	0.030
5.2	0.080
7.7	0.122
10.7	0.126
17.1	0.194
17.6	0.205
19.6	0.243
20.7	0.264
23.2	0.287
27.1	0.316
28.6	0.331
30.7	0.405
31.2	0.436
31.7	0.436
32.2	0.475
35.1	0.490
41.2	0.554
45.6	0.617
47.1	0.701
47.6	0.736
48.7	0.784
55.6	0.860
57.6	0.883
58.7	0.909
59.2	0.916
64.6	0.953
68.7	0.996
70.7	1.026
71.7	1.068
78.7	1.110
80.2	1.132
83.1	1.186
91.1	1.382
91.6	1.390
101.6	1.532

Table T5. Age-depth data based on shipboard bio-stratigraphic horizons, Hole 1081A.

Depth (m)	Age (Ma)
4.20	0.09
21.93	0.26
31.07	0.46
40.81	0.60
54.00	0.83
63.59	0.96
71.25	1.10
107.88	1.67

Note: Shipboard biostratigraphic horizons from Shipboard Scientific Party, 1998e.